








Helium-isotope constraints on palaeoceanographic change and sedimentation rates during precession cycles (Cenomanian Scaglia Bianca Formation, central Italy)

JAMES R. LUCAS* , SIETSKE J. BATENBURG† , DARREN J. HILLEGONDS* ,
JENNIFER C. MABRY‡ , HUGH C. JENKYNs* , CHRIS J. BALLENTINE*  and
STUART A. ROBINSON* 

*Department of Earth Sciences, University of Oxford, South Parks Road, Oxford OX1 3AN, UK
(E-mail: stuart.robinson@earth.ox.ac.uk)

†Departament de Dinàmica de la Terra i de l'Oceà, Universitat de Barcelona, Martí i Franquès, s/n,
Barcelona 08028, Spain

‡Section of Isotope Hydrology, International Atomic Energy Agency (IAEA), Vienna International
Centre, PO Box 100, Vienna A-1400, Austria

Associate Editor – Ying Zhou

ABSTRACT

For much of the pelagic sedimentary record, time control is limited to the resolution of precession cycles (*ca* 20 kyr): the Milankovitch parameter that forms the most detailed metronome for the Cenozoic and Mesozoic Eras. The influence of precession is often detected in lithological alternations, where the duration represented by individual lithologies is not well constrained. Here the novel technique of extraterrestrial helium abundance ($^3\text{He}_{\text{ET}}$) is used to investigate the sedimentation dynamics and palaeoceanography within individual precessional cycles. High-resolution $^3\text{He}_{\text{ET}}$ timescales were produced for four precession cycles from the rhythmically bedded Scaglia Bianca Formation, a sequence of Upper Cretaceous (Cenomanian) deep-marine pelagic limestones from central Italy that are well characterized by cyclostratigraphy. Using $^3\text{He}_{\text{ET}}$ concentrations as a proxy for sedimentation rate allows instantaneous sedimentation rates and organic-carbon mass accumulation rates to be calculated for each bed within a precession cycle. Eccentricity is known to modulate the amplitude of precession forcing, and precession cycles deposited under eccentricity maxima and minima were selected for comparison. Lithological changes through these chert–(black shale)–limestone cycles are explained using the concept of ‘palaeoenvironmental thresholds’; these timescale calculations indicate that when the amplitude of precessional insolation forcing was greatest (at eccentricity maxima) the palaeoenvironmental system spent longer in the more nutrient-rich environment under which siliceous and organic-rich sediments were deposited, reflecting increased time spent above a ‘threshold’ insolation level. Estimates of primary productivity are relatively elevated for organic-rich beds. An increase in the flux of terrestrial helium ($^4\text{He}_{\text{terr}}$) during the deposition of cherts may have been coincident with an increase in terrestrially derived nutrients. The presented results indicate great potential for the use of $^3\text{He}_{\text{ET}}$ to understand past oceanographic, climatic and sedimentological processes at high temporal resolution.

Keywords Age model, Cenomanian, helium, IDP, pelagic environment, precession.

INTRODUCTION

Orbitally forced, periodic changes in lithology and geochemistry have been identified in sediments from the Palaeozoic to the Quaternary (e.g. Hinnov, 2013) as repeated alternations of lithologies. Although cyclostratigraphy offers considerable insight into the overall duration and bundling of these cycles, the smallest ‘increment’ of time that can be explored using cyclostratigraphy is the period of the shortest cycle: the short precession cycle, *ca* 19 kyr in modern sediments (Hinnov, 2013). For precession cycles themselves to be identifiable, a distinct change in either lithology or geochemistry must occur within them, but so far the tools to quantify how fast these changes occur, or how long they last, have been largely lacking for sediments older than the Quaternary (but see recent work by Blard *et al.*, 2023 on the origin of limestone–marl cycles).

Of particular interest to this study is how forcing functions of different amplitudes (i.e. precession cycles at different points within a modulating short eccentricity cycle) affect how ‘strongly’ the environment responds: does the lithology change more dramatically, and does the division of time represented by different lithologies change? To address these questions, records of the same cycle in different parts of a basin are examined to investigate how the same forcing mechanisms affected sections deposited under slightly different environmental regimes. Deciphering the division of time within a precession cycle will also help to understand how the essentially sinusoidal-shaped insolation curve may be represented in the sedimentary record.

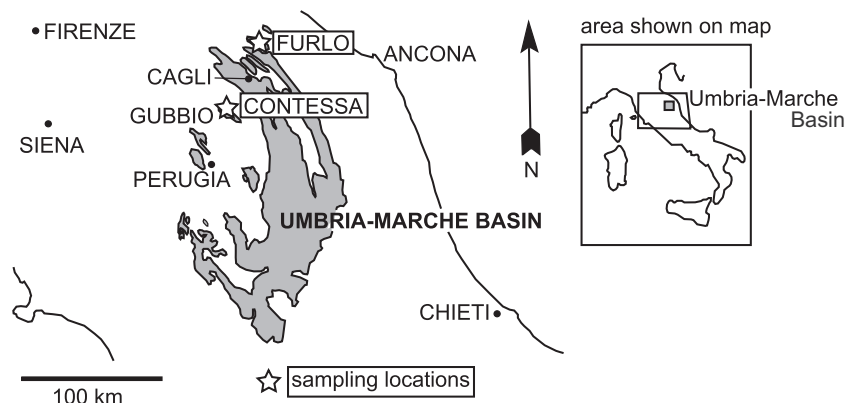
Interplanetary dust particles (IDPs) contain extremely elevated $^3\text{He}/^4\text{He}$ ratios (*ca* $2.4 \pm 0.3 \times 10^{-4}$, Nier & Schlutter, 1990, 1992) compared to terrestrial materials (*ca* 2 to 6×10^{-8} , Farley, 2001). IDPs are supplied to pelagic sediments at essentially constant rates over geologically short intervals of time (on the order of hundreds of kyr, Farley, 2001). Consequently, slowly depositing pelagic sediments contain relatively high concentrations of ^3He due to low rates of biogenic and terrigenous sediment accumulation, thereby leading to relatively high abundances of IDPs and detectable $^3\text{He}_{\text{ET}}$ concentrations above the terrestrial background (Ozima *et al.*, 1984). With a constant flux of IDPs, it is thus possible to use the extraterrestrial ^3He ($^3\text{He}_{\text{ET}}$) concentrations to calculate an

instantaneous sedimentation rate on a bed-by-bed basis (Takayanagi & Ozima, 1987; Farley, 2001) and, consequently, produce high-resolution timescales within precession cycles. Four precession cycles are examined within the Cenomanian (Upper Cretaceous) deep-marine pelagic Scaglia Bianca Formation of Marche–Umbria, Italy, identified using the cyclostratigraphic analysis of Batenburg *et al.* (2016). The light-coloured Scaglia Bianca sediments primarily comprise planktonic foraminifera set in a matrix of solution-welded nannofossils and carbonate-replaced radiolaria; *ca* 20 cm thick carbonate intervals are interbedded with *ca* 3 cm darker cherts in which siliceous microfossils are better preserved (Cresta *et al.*, 1989). The rhythmic bedding of the Scaglia Bianca has been long recognized, with many studies linking the alternations of limestone and black chert (and, in some cycles, black shale) to Milankovitch cycles. Specifically, *ca* 20 cm packets composed of *ca* 17 cm of limestone and *ca* 3 cm of chert (in some cases with *ca* 0.5 cm of black shale) are attributed to *ca* 21 kyr precession cycles (Arthur & Premoli Silva, 1982; de Boer, 1982; Schwarzer, 1994; Beaudoin *et al.*, 1996; Mitchell *et al.*, 2008; Lanci *et al.*, 2010; Sprovieri *et al.*, 2013; Batenburg *et al.*, 2016; Laurin *et al.*, 2016; Gambacorta *et al.*, 2019). Both short and long eccentricity modulate the amplitude of these precession cycles; and although cycles containing black cherts were suggested to correspond to eccentricity minima by Lanci *et al.* (2010), these cycles are more generally thought to have occurred during eccentricity maxima (Mitchell *et al.*, 2008; Batenburg *et al.*, 2016; Laurin *et al.*, 2016).

MATERIALS AND METHODS

Four precession cycles within the upper part of the Upper Cretaceous Scaglia Bianca Formation, collected from two localities in the Umbria–Marche Basin (quarried sections at Furlo and Contessa; Fig. 1), were studied in detail. Both of these sections expose the overlying metre-thick black shale and radiolarian sand of the Bonarelli Level (Cenomanian–Turonian boundary), which is the local lithological expression of Oceanic Anoxic Event 2 and constitutes a distinctive marker bed. The Scaglia Bianca has been subdivided by some workers into four members (Coccioni & Galeotti, 2003); sampled precession cycles were drawn from the topmost unit, the

Fig. 1. Location of the Umbria–Marche Basin in central Italy showing sampling locations. Shaded outcrop area represents Triassic–Eocene age basin fill (after Arthur & Premoli Silva, 1982).



‘Greyish Member’, which begins stratigraphically above the mid-Cenomanian positive $\delta^{13}\text{C}$ excursion (MCE = mid-Cenomanian Event) and, in Furlo, contains black chert and thin black shale layers interpreted as reflecting the enhanced sensitivity of the sedimentary regime post-MCE to changes in the hydrological cycle (Coccioni & Galeotti, 2003; Turgeon & Brumsack, 2006; Gambacorta *et al.*, 2019). Black cherts are not underlain by black shale layers in the Contessa section, indicating a subtle difference in the environmental regimes under which the two otherwise very similar sections were deposited. Figure 2 shows the stratigraphic position of the three sub-Bonarelli Level cycles sampled from the Furlo section (Furlo Cycles A, B and C). In addition, a cycle from Contessa (Contessa Cycle B) was sampled at the same stratigraphic position as Furlo Cycle B (Fig. 3). An additional cycle from the Scaglia Bianca above the Bonarelli Level at Furlo (Furlo Cycle D) was sampled solely for use in the calculation of background flux (see *Discussion* section).

Detailed sedimentary logs were created for each precession cycle with samples collected in stratigraphic continuity. For marls, shales and cherts occurring in thin *ca* 1 cm beds, this methodology required sampling the entirety of each bed. Thick limestone beds were sampled as blocks and usually homogenized in 5 cm sections. Sampling at a higher resolution than this through the limestone was thought to be unnecessary because the limestones are well bioturbated and therefore already likely to be homogenous on this scale (Coccioni & Galeotti, 2003; Gambacorta *et al.*, 2014).

A Rock-Eval 6 [Vinci Technologies, Nanterre, France] was used to determine Total Organic Carbon (TOC) content, inorganic (carbonate)

content (mineral carbon), Hydrogen Index (HI), Oxygen Index (OI) and T_{max} of samples (see Behar *et al.*, 2001). Carbonate content was calculated by multiplying mineral carbon by 8.333. For some samples with very low TOC, HI, OI and T_{max} were measured in decarbonated sample material (see Supplementary Information). Errors ($\pm 1\sigma$) on Rock-Eval measurements (as calculated from 41 analyses of an internal standard, previously calibrated to international standards) are $\pm 0.04\%$ for TOC, $\pm 0.10\%$ for mineral carbon, $\pm 17 \text{ mg HC g}^{-1} \text{ TOC}$ for Hydrogen Index, $\pm 4 \text{ mg CO}_2 \text{ g}^{-1} \text{ TOC}$ for Oxygen Index and $\pm 2^\circ\text{C}$ for T_{max} .

Following Patterson & Farley (1998), samples were powdered, decarbonated using 10% acetic acid, rinsed in deionized water and dried overnight, prior to measurements of helium concentration. The carbonate fraction ($\text{CaCO}_3\%$) and non-carbonate fraction (NCF) were calculated from pre-decarbonation and post-decarbonation weight, with decarbonation replicates indicating 1σ variability of up to 2%. Decarbonated sample powders were heated using a Fusions Diode 0.970 Laser Stepped Heating System (Teledyne CETAC, Omaha, NE, USA). Following this process, gas released was exposed to a cold finger containing a mixture of 5 g activated charcoal and 12 g 5 Å molecular sieves cooled with liquid nitrogen, before being further purified using MP10 getters (SAES st101 alloy, as provided with the commercial noble-gas prep line). Helium was then separated using a cryogenic trap containing activated charcoal held between *ca* 10 and 90 K (Janis Research Company, Inc., Wilmington, MA, USA). Helium concentration was measured on a HELIX SFT mass spectrometer (ThermoFisher Scientific, Waltham, MA, USA), and helium abundances and isotopic ratios were determined by comparison

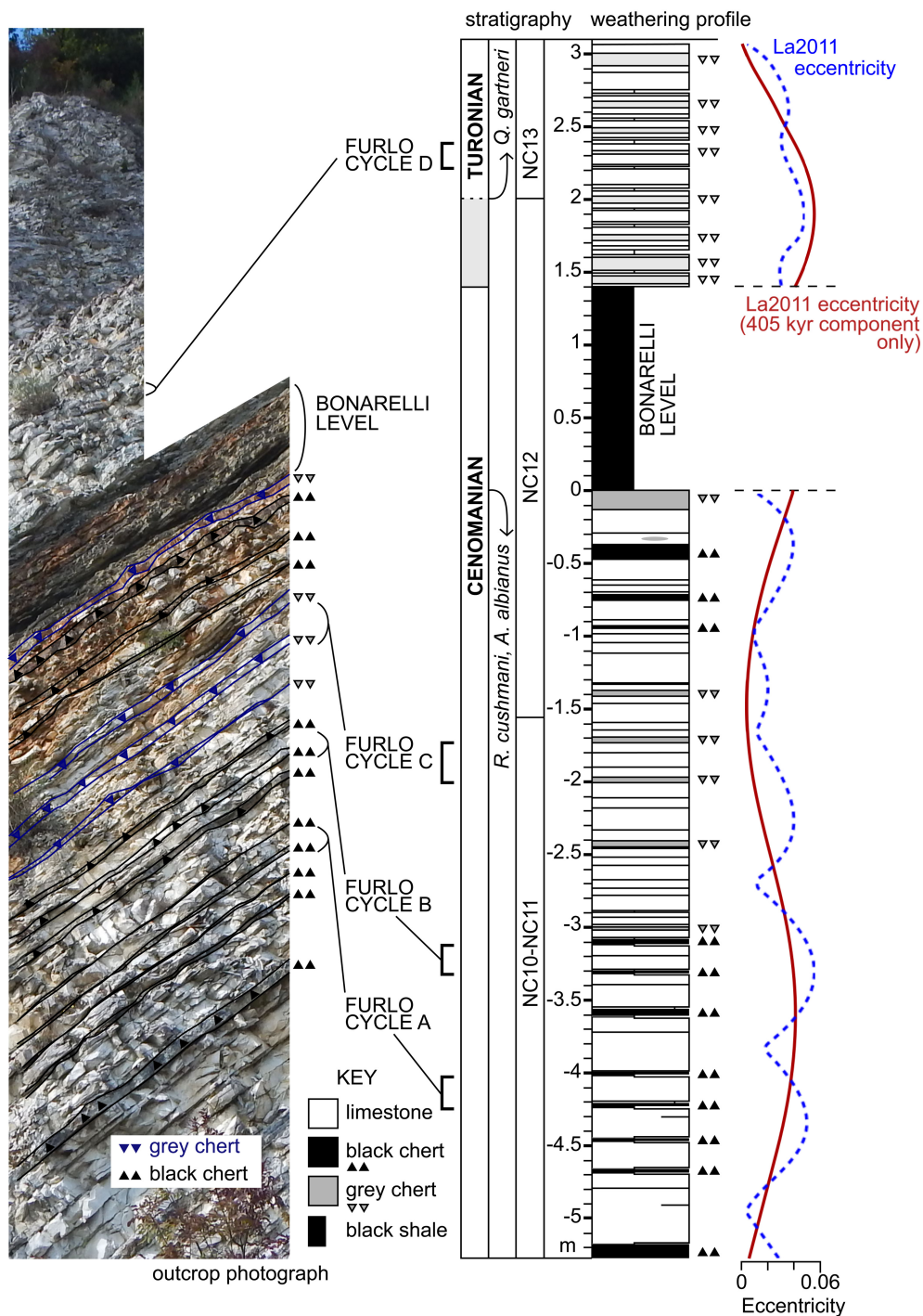
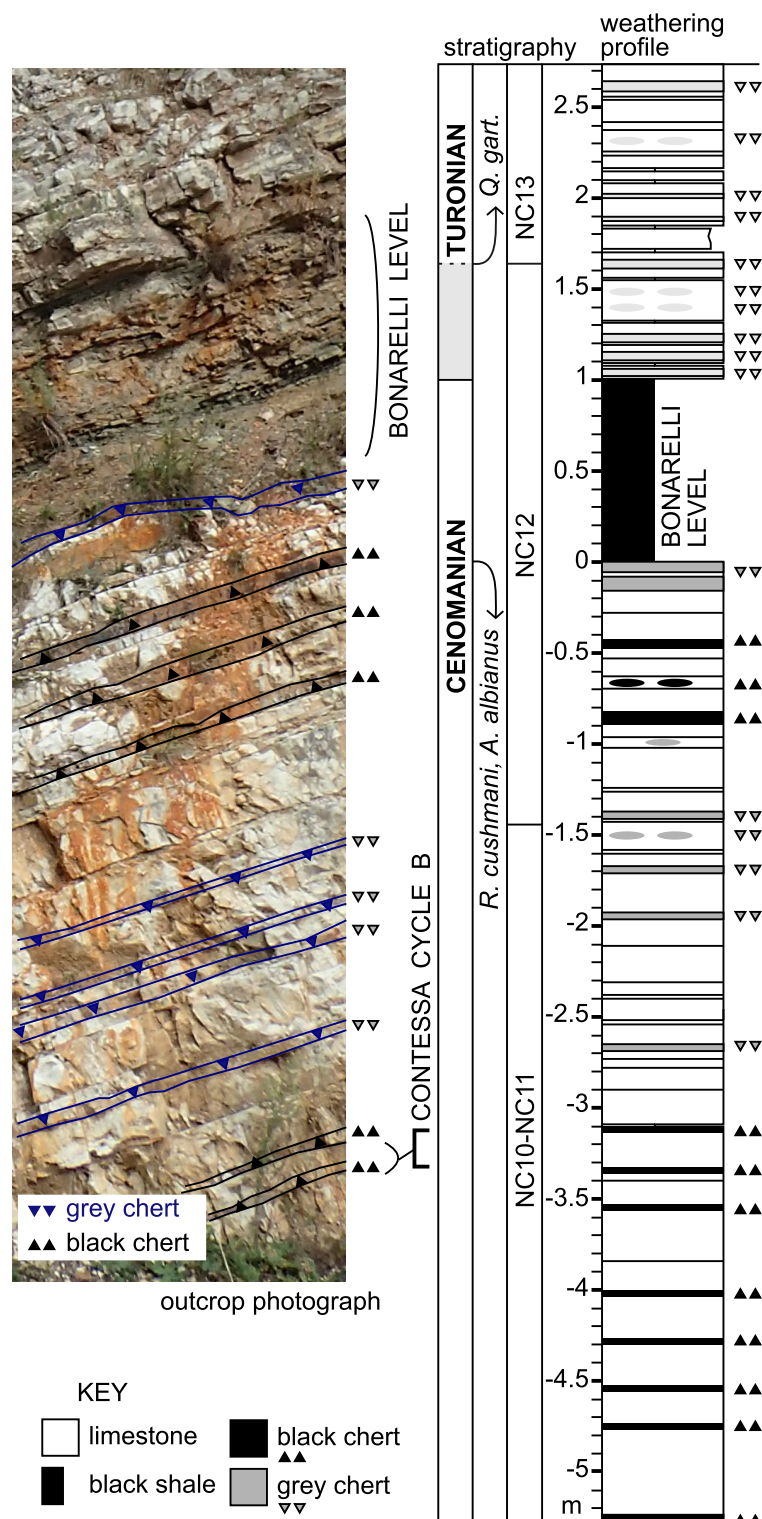


Fig. 2. Position of studied cycles within the Furlo section. Cyclostratigraphic interpretations are from Batenburg *et al.* (2016); the blue dashed curve represents one of their tuning models ('tuning 2') to La2011 eccentricity (Laskar *et al.*, 2011a,b) of the Umbria–Marche succession, the red curve indicates just the 405 kyr eccentricity component. Nannofossil zones follow Tsikos *et al.* (2004) and Batenburg *et al.* (2016). The Cenomanian–Turonian boundary is placed following the interpretation of Gambacorta *et al.* (2015), represented by a solid line in the stratigraphic column. It should be noted that an alternative position of the Cenomanian–Turonian boundary is advanced by Batenburg *et al.* (2016), presented as a dashed boundary, with a grey bar across the interval of uncertainty. Cycles A and B were deposited during times when the amplitude of eccentricity was relatively high; Cycle C was deposited when eccentricity amplitude was relatively low.

Fig. 3. Position of studied cycle within the Contessa section. Nannofossil zones follow Tsikos *et al.* (2004) and Batenburg *et al.* (2016). The Cenomanian–Turonian boundary is placed following the interpretation of Gambacorta *et al.* (2015), represented by a solid line in the stratigraphic column. It should be noted that an alternative position of the C–T boundary is advanced by Batenburg *et al.* (2016), presented as a dashed boundary, with a grey bar across the interval of uncertainty.



with air-shots of a known volume analysed using the same procedure as the samples, following McGee *et al.* (2010). Analytical errors were *ca* 4% of measured ^4He concentrations and *ca* 9% for measured ^3He concentrations. Typical blank values

for ^4He were *ca* 4% and *ca* 5% for ^3He . Helium produced following re-heating of fused samples was at blank levels.

Reproducibility of ^3He in repeat measurements was typically worse than analytical error,

due to the 'nugget effect' of a relatively small number of extraterrestrial ^3He -rich particles in each sample aliquot (Patterson & Farley, 1998; Farley, 2001). Errors of 20% were applied to measured ^3He concentrations to reflect this effect: the reproducibility of ^3He concentration in sample replicates from Umbria–Marche sections were found to approximately match a Gaussian distribution with 1σ *ca* 20%. The helium content of each sample was measured twice, with additional measurements made if ^3He concentrations of duplicates were not within error of one another. Outliers were subsequently identified using Chauvenet's Criterion; *ca* 13% of all measurements were identified as outliers in this manner.

The non-carbonate fraction (NCF) calculated during decarbonation was used to convert measured He concentration ($[\text{He}]/\text{NCF}$) into He concentration in bulk sediment: $[\text{He}]_{\text{bulk}} = ([\text{He}]/\text{NCF})_{\text{measured}} \times \text{NCF}$. The extraterrestrial ^3He component ($^3\text{He}_{\text{ET}}$) was deconvolved from the measured ^3He concentration and the $^3\text{He}/^4\text{He}$ ratio using a two-component mixing model: $[^3\text{He}_{\text{ET}}] = [^3\text{He}_{\text{observed}}] \times (^4\text{He}/^3\text{He}_{\text{observed}} - ^4\text{He}/^3\text{He}_{\text{terrestrial}}) / (^4\text{He}/^3\text{He}_{\text{ET}} - ^4\text{He}/^3\text{He}_{\text{terrestrial}})$ (Patterson & Farley, 1998). End-member composition values used were: $^3\text{He}/^4\text{He}_{\text{ET}} = 2.4 \times 10^{-4}$ (average value of interplanetary dust particles measured in the atmosphere, Nier & Schluter, 1990, 1992), and $^3\text{He}/^4\text{He}_{\text{terr}} = 3 \times 10^{-8}$ (average terrestrial crust, Farley, 2001; Farley *et al.*, 2012). The differences in extraterrestrial ^3He fraction calculated using $^3\text{He}/^4\text{He}_{\text{terr}}$ between average crustal ranges of 2 to 6×10^{-8} were less than 20% for the majority of samples.

RESULTS

Sedimentology

A facies numbering scheme, developed for the Scaglia Bianca by Gambacorta *et al.* (2014), was adopted to describe lithological change through the studied cycles (Fig. 4). Cycles of the Scaglia Bianca are easily picked out by eye as alternations of limestone and chert. At Furlo, *ca* 3 cm thick generally tabular black chert beds are typically underlain by a *ca* 0.5 cm layer of black shale (as in Furlo Cycles A and B), whereas grey chert beds are not (as in Furlo Cycle C). Chert and shale lithologies are laterally continuous across the quarry face at Furlo and Contessa, but are slightly variable in thickness. Contacts

between lithologies within cycles are sharp; these may be diagenetic fronts.

The bulk of all studied cycles comprise homogenous limestone (facies 'A1' and 'A2', 'homogenous marly limestone' and 'homogenous limestone', respectively). These limestones are *ca* 1 to 5 cm or *ca* 3 to 40 cm thick layers, respectively, composed of planktonic foraminifera (with rare benthic foraminifera) in a micritic matrix made up of solution-welded coccoliths with minor amounts of clay (Gambacorta *et al.*, 2014). The diffuse mottling observed through this lithology has been interpreted as due to homogenization by bioturbation (Gambacorta *et al.*, 2014). Limestones below the black shales commonly contain organic-rich laminae (facies 'A4', 'alternating and organic-rich laminasets'), ranging in thickness from less than 1 mm to about 1 cm, which appear in thin-section as a concentration of flakes of organic matter (Fig. 5A).

Chert beds vary in colour through the Scaglia Bianca and may be black (facies 'G4'), grey (facies 'G3') or even pink; this colour change is interpreted as reflecting the oxidation state at the time of their formation (Gambacorta *et al.*, 2014). The granular texture that these cherts display in hand specimen is created by 'ghost' radiolarians, which sit in a matrix of micro-quartz (Fig. 5B). Chert layers through the Scaglia Bianca range between 0.5 cm and 20 cm in thickness. In some cherts, millimetre-scale lamination is clearly visible in hand-specimen formed by alternating layers of silt-sized to sand-sized radiolaria and finer laminae containing more clay and organic matter (Gambacorta *et al.*, 2014).

Contacts between chert and neighbouring lithologies are abrupt and may be plane-parallel or undulose. Examination of a limestone bed immediately above a chert revealed replacement of both calcitic and siliceous microfossils by chalcedonic quartz; more radiolarians were present in this bed than in the 'homogenous limestone' above, perhaps due to better preservation (Fig. 5C). A thin-section taken across the boundary between a black chert and underlying black shale indicates that between these two lithologies is *ca* 0.5 mm of matrix composed of interfingering microcrystalline calcite (immediately above the black shale) and microcrystalline silica (immediately below the black chert); this matrix is devoid of the abundant microfossils characteristic of both black shale and black chert and also largely devoid of organic matter (Fig. 5E and F).

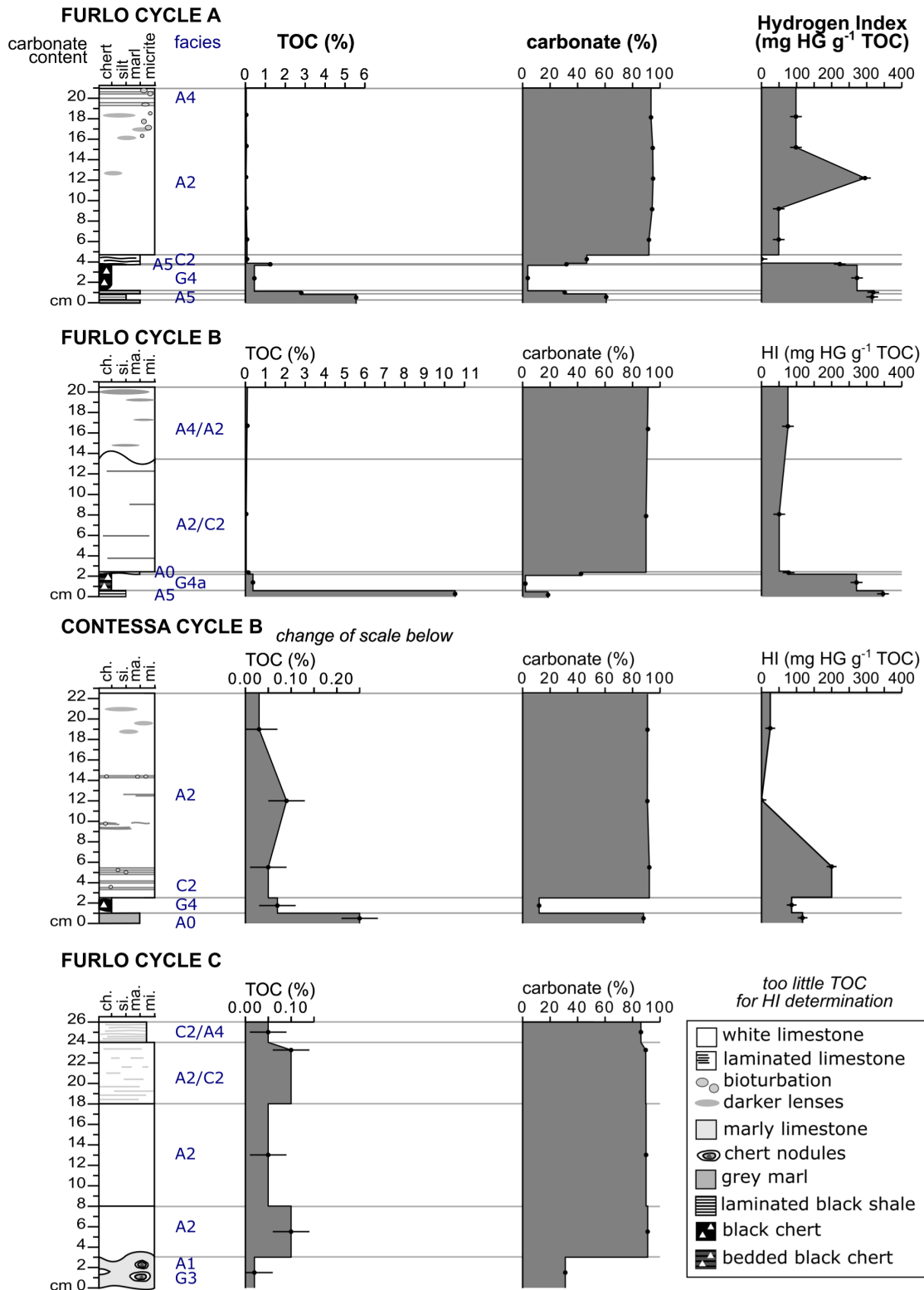


Fig. 4. Lithology, total organic carbon content and carbonate content for four Scaglia Bianca precession cycles. Number codes for facies are from Gambacorta *et al.* (2014); A0 = marl, A1 = homogenous marly limestone, A2 = homogenous limestone, A4 = alternating micritic and organic-rich lamina-sets, A5 = black shale, C2 = limestone with plane-parallel laminations, G3 = grey chert, G4(a) = black chert (bedded). Sampling positions are represented by points on the plot. Error bars on plotted points represent analytical uncertainties.

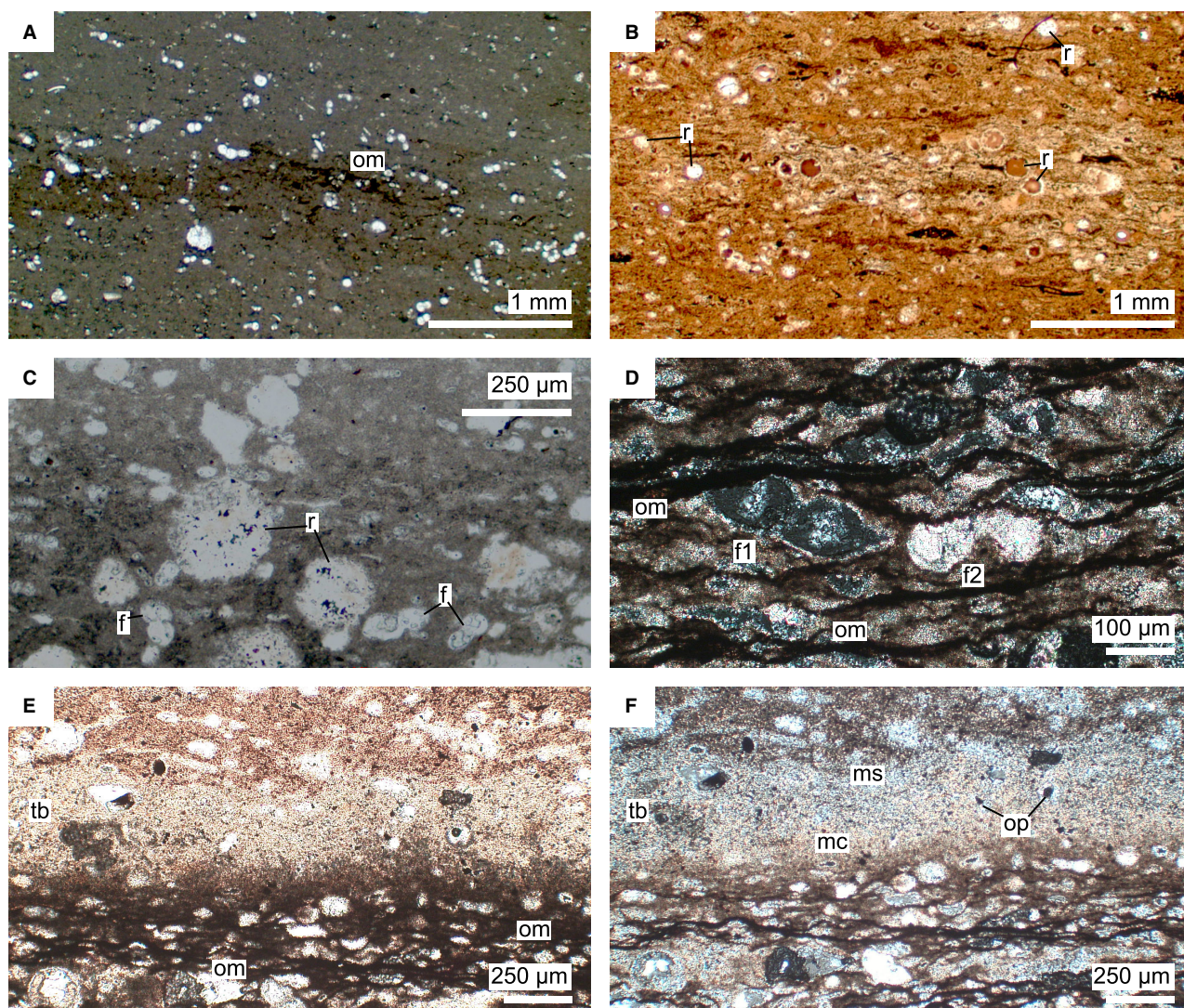


Fig. 5. Thin-section images of precession cycle lithologies. (A) Organic-rich lamina (om) in a limestone bed (facies A4) under plane-polarized light. (B) Black chert bed (facies G4) with 'ghost' radiolarians (r), (plane-polarized light). (C) Silicified radiolarians (r) and foraminifera (f) in a micritic matrix (facies C2), made up of solution-welded nanofossils (plane-polarized light). (D) Black shale bed (facies A5) under crossed polars. Stringers of organic matter (om) form a pervasive fabric parallel to bedding. Equatorial view through two coiled planktonic foraminifera infilled with silica (f1) and large crystals of calcite spar (f2). (E) Section across the boundary between black shale (base) and black chert (top), (plane-polarized light, younging direction upward). Abundant organic matter (om) can be seen in the black shale, with rather less in the black chert, and very little in the *ca* 500 µm transitional band (tb) between them. This band is also largely devoid of microfossils. (F) Boundary section between black shale and black chert under crossed polars. The transitional band is made up of interfingering microcrystalline calcite (mc) and microcrystalline silica (ms) and contains relatively large euhedral opaque crystals (op).

Furlo Cycles A and B contain black shales (facies 'A5'). These lithologies are very dark in colour and have fine papery lamination; detailed analysis by Gambacorta *et al.* (2014) revealed highly variable TOC and carbonate content from

lamina to lamina. Enrichments in TOC up to 10% were measured in this study; underscoring the variability of TOC content within black shale beds, TOC values of up to 20% in sub-Bonarelli black shales were recorded by Jenkyns *et al.*

(2007), but Owens *et al.* (2017) did not record values higher than 5%. In thin-section, long stringers of organic matter form a pervasive fabric parallel to the bedding plane (Fig. 5D). Unlike the black shales of the Bonarelli Level itself, which are devoid of carbonate, the Cenomanian black shales associated with precession cycles (termed here 'sub-Bonarelli black shales') have moderately high carbonate contents, from 18 to 87%. These sub-Bonarelli black shales contain both foraminiferal and radiolarian microfossils, typically infilled with silica (but locally carbonate) cements, in a sparry ground-mass containing flecks of organic matter and opaque, euhedral minerals (most likely pyrite). At Furlo, black-shale layers range from less than 1 cm to about 5 cm in thickness. Cycles at Contessa do not contain black shales, although the black chert of Contessa Cycle B is underlain by a marl (facies 'A0') that is distinctly elevated in TOC content (0.25%) from the underlying limestone (0.03 to 0.09%).

In the Scaglia Bianca precession cycles, the predominance of organic matter with Type II Hydrogen Index (HI) values suggests a marine source for the major part of the organic carbon (Fig. 6). Black shales, black cherts and marls typically have higher Hydrogen Indices than limestones, likely reflecting enhanced organic-matter preservation under low-oxygen conditions. Hydrogen Index values from Contessa samples are uniformly lower than in those from Furlo, in parallel with the overall lower organic-carbon content in this section. It is possible that the two locations experienced

different burial histories/thermal maturation. A study of vitrinite reflectance across sediments in another part of the Apennine fold-and-thrust belt indicates that large changes in thermal history are possible between relatively nearby sites in this setting (Caricchi *et al.*, 2015); however, T_{\max} values measured in this study were not significantly different between the two sites (T_{\max} = 325 to 451°C at Furlo and 330 to 442°C at Contessa). If not due to differing thermal histories, these differences may instead suggest less favourable conditions for organic-matter preservation at Contessa: the observed pattern in Hydrogen Index values are consistent with more oxidizing conditions in the water column during deposition, or in the sediments during early diagenesis. These observations are, however, also consistent simply with deeper and more pervasive weathering at the Contessa site.

Helium concentration

The measured concentrations (in bulk sediment) of extraterrestrial ^3He and terrestrial ^4He through the studied precession cycles are presented in Fig. 7. The average concentration of $^3\text{He}_{\text{ET}}$ in limestones is similar across all Furlo cycles: $ca\ 1.8 \pm 0.2$ to $2.4 \pm 1.1 \times 10^{-14}\ \text{cc g}^{-1}$, with a somewhat lower concentration ($ca\ 0.8 \pm 0.2 \times 10^{-14}\ \text{cc g}^{-1}$) measured in the limestone of the Contessa cycle (uncertainties reflect intra-bed variability).

The $^3\text{He}_{\text{ET}}$ concentration does not vary significantly through Furlo Cycle C. By contrast, the black shales of Furlo Cycles A and B display

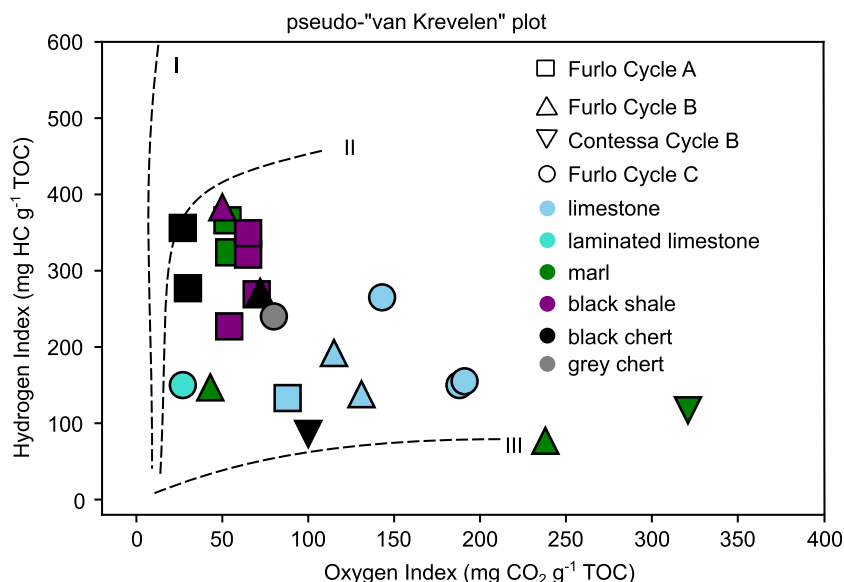


Fig. 6. Van Krevelen-type plot (after Espitalié *et al.*, 1985) showing the variation of organic-matter types with lithology in the studied Scaglia Bianca precession cycles.

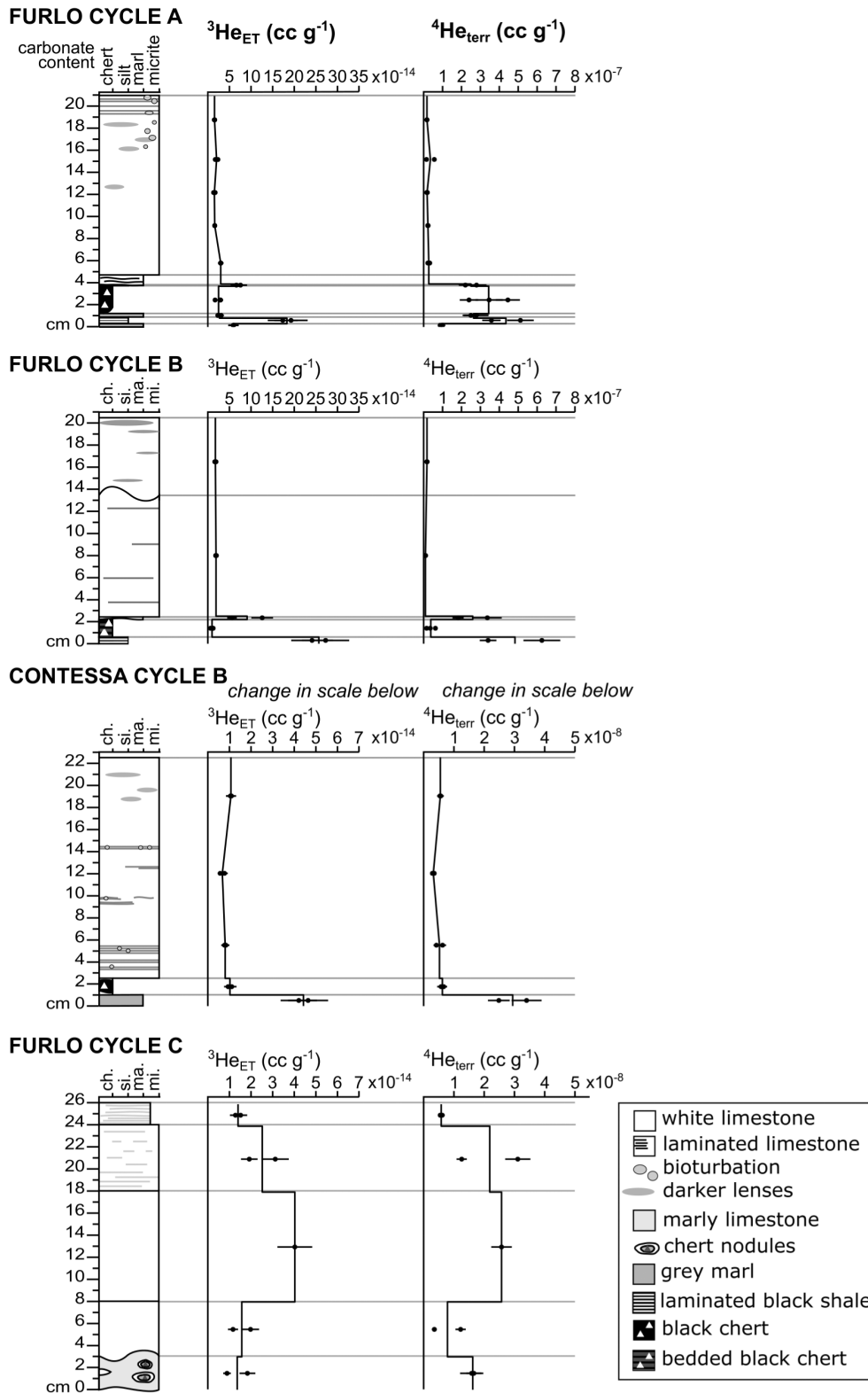


Fig. 7. Extraterrestrial ^3He and terrestrial ^4He concentration through the studied precession cycles. Data points represent individual measurements; vertical lines are average values. Error bars on $^3\text{He}_{\text{ET}}$ (cc g^{-1}) represent 20% reproducibility error due to the nugget effect; error bars on $^4\text{He}_{\text{terr}}$ derive from analytical error.

markedly elevated concentrations of $^3\text{He}_{\text{ET}}$, with average concentrations of $1.8 \pm 0.3 \times 10^{-13} \text{ cc g}^{-1}$ and $2.6 \pm 0.4 \times 10^{-13} \text{ cc g}^{-1}$, respectively, whereas the marl of Contessa Cycle B has a more modestly elevated $^3\text{He}_{\text{ET}}$ concentration of $4.4 \pm 0.6 \times 10^{-14} \text{ cc g}^{-1}$. Errors on average $^3\text{He}_{\text{ET}}$ concentrations in single horizons, i.e. black shale and marl beds, are propagated from 20% differences on $^3\text{He}_{\text{ET}}$ concentrations in individual samples, which are larger than the standard deviation of measurements (Fig. 8).

The black chert beds in these three cycles do not display this $^3\text{He}_{\text{ET}}$ enrichment; average $^3\text{He}_{\text{ET}}$ concentration in these black cherts ranges from $ca\ 1.0 \pm 0.3$ to $2.5 \pm 0.7 \times 10^{-14} \text{ cc g}^{-1}$, comparable to concentrations measured in the limestones. The large uncertainties on these averages reflect the fact that standard deviation of measured $^3\text{He}_{\text{ET}}$ concentrations in chert beds is larger than would be expected due to the predicted 20% 'nugget effect' uncertainty. Fast sedimentation rates and high non-carbonate content in cherts resulted in relatively low area-time products represented by each sample, despite a compensatory increase in sample mass, which may have made the nugget effect more pronounced.

The concentration of terrestrial ^4He also varies across three of the precession cycles. Typically, the lowest average concentrations of $^4\text{He}_{\text{terr}}$

occur in limestones, though the actual values vary from cycle to cycle (between $ca\ 0.5 \pm 0.1$ and $2.5 \pm 1.2 \times 10^{-8} \text{ cc g}^{-1}$). Over Furlo Cycle C, however, there appears to be no significant variation in $^4\text{He}_{\text{terr}}$ concentration. By contrast, spikes in the concentration of $^4\text{He}_{\text{terr}}$ are observed in the black shale and marl beds of Furlo Cycles A and B and Contessa Cycle B, average $^4\text{He}_{\text{terr}}$ concentrations being $4.4 \pm 1.1 \times 10^{-7} \text{ cc g}^{-1}$, $4.8 \pm 2.0 \times 10^{-7} \text{ cc g}^{-1}$ and $2.9 \pm 0.6 \times 10^{-8} \text{ cc g}^{-1}$, respectively. The black cherts in Furlo Cycle A and, to a lesser degree, Furlo Cycle B also contain a noticeably elevated concentration of $^4\text{He}_{\text{terr}}$ relative to the limestones; average concentrations from chert beds are $3.4 \pm 1.0 \times 10^{-7} \text{ cc g}^{-1}$ and $3.8 \pm 2.3 \times 10^{-8} \text{ cc g}^{-1}$, respectively. As no 'nugget effect' is expected to impact the measured concentration of $^4\text{He}_{\text{terr}}$, the error on average $^4\text{He}_{\text{terr}}$ within a bed derives simply from the standard deviation of individual measurements.

DISCUSSION

Background flux

Before timescales can be constructed from $^3\text{He}_{\text{ET}}$ concentration measurements, the background flux of extraterrestrial ^3He must be determined. Background flux, F ($\text{cc cm}^{-2} \text{ kyr}^{-1}$), can be calculated from measured $^3\text{He}_{\text{ET}}$ concentration, $[^3\text{He}_{\text{ET}}]$ (cc g^{-1}), over intervals where mass accumulation rate, α ($\text{g cm}^{-2} \text{ kyr}^{-1}$), can be calculated by independent means using the equation: $F = [^3\text{He}_{\text{ET}}] \times \alpha$ (Takayanagi & Ozima, 1987).

The primary concern of this study was the comparison of sedimentation rates and the division of time within precession cycles; for this reason, a background flux (F_{cycle}) value unique to each cycle was calculated, and variations in $[^3\text{He}_{\text{ET}}]$ within each cycle used to derive variable sedimentation rates. Each cycle provided a 'snapshot' of $^3\text{He}_{\text{ET}}$ background flux over spans of $ca\ 20 \text{ kyr}$, much shorter than the 100 kyr dynamical lifespan of $^3\text{He}_{\text{ET}}$ -bearing interplanetary dust particles in the Solar System (Farley, 2001). In this way, this method of sedimentation rate calculation avoided introduction of the variability inherent in applying a single average background flux calculated across the $ca\ 400 \text{ kyr}$ interval between the deposition of Cycle A and Cycle C (see Farley *et al.*, 2012).

Background flux (F_{cycle}) over a precession cycle was calculated: $F_{\text{cycle}} = [^3\text{He}_{\text{ET}}]_{\text{avg}} \times \alpha^*$. An

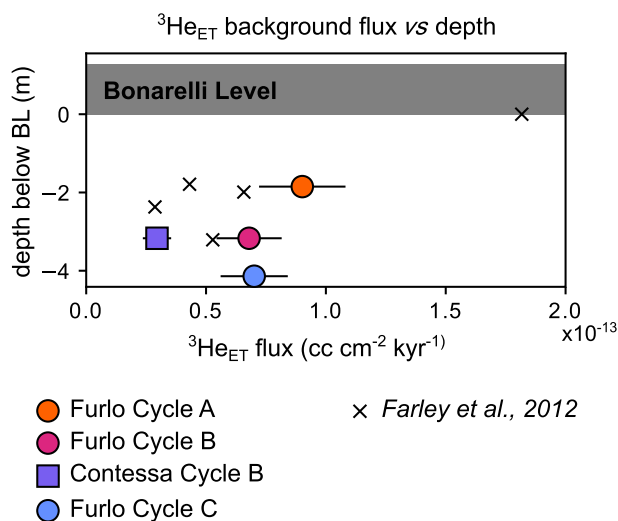


Fig. 8. Background flux against depth, calculated in each studied precession cycle. Error bars on background flux values are a result of error propagation from the measurements that went into their calculation, including the 20% uncertainty on $^3\text{He}_{\text{ET}}$ concentration from inter-sample variability.

average helium concentration over the cycle ($[^3\text{He}_{\text{ET}}]_{\text{avg}}$) was derived from a proportional average of the helium concentrations measured in the cycle's constituent beds: $[^3\text{He}_{\text{ET}}]_{\text{avg}} = \Sigma([^3\text{He}_{\text{ET}}]_{\text{bed}} \times \text{bed thickness}) / \text{cycle thickness}$. The calculation of $[^3\text{He}_{\text{ET}}]_{\text{avg}}$ was only performed once, but multiple replicate measurements were made when determining the $^3\text{He}_{\text{ET}}$ content of individual beds.

Sedimentation mass accumulation rate (α^* ; $\text{g cm}^{-2} \text{ kyr}^{-1}$) was calculated for each cycle by assuming that each cycle spans 21 kyr: $\alpha^* = (\text{cycle thickness} \times \text{average density}) / (\text{cycle duration})$. This assumption of the time spanned by each cycle is not without caveats. Although, in the Scaglia Bianca, a large body of evidence links the chert–limestone cycles to precession (Arthur & Premoli Silva, 1982; de Boer, 1982; Mitchell *et al.*, 2008; Lanci *et al.*, 2010; Batenburg *et al.*, 2016; Gambacorta *et al.*, 2019), the ‘21 kyr precession cycle’ is, itself, an average of the four precession cycle periods that occurred through the Cenomanian (23.03 ± 0.37 kyr, 21.79 ± 0.34 kyr, 18.53 ± 0.29 kyr and 18.68 ± 0.30 kyr), and different precessional periods may have dominated at different points along the long eccentricity cycle (Berger *et al.*, 1992; Berger & Loutre, 1994; Laskar *et al.*, 2004, 2011a; Waltham, 2015; Zeeden *et al.*, 2015). The assumption of a 21 kyr time span impacts calculated sedimentation rates and durations within the constructed $^3\text{He}_{\text{ET}}$ timescales, with a knock-on effect on calculated organic-carbon mass accumulation rates and fluxes of terrestrial ^4He . Were the cycles to have spanned a different time interval, the relative sedimentation rates within cycles would still stand, though the exact numbers would vary.

The following background flux values were calculated for each cycle (Fig. 8): $7.0 \pm 1.4 \times 10^{-14} \text{ cc cm}^{-2} \text{ kyr}^{-1}$ over Furlo Cycle A, $6.8 \pm 1.4 \times 10^{-14} \text{ cc cm}^{-2} \text{ kyr}^{-1}$ over Furlo Cycle B, $3.0 \pm 0.6 \times 10^{-14} \text{ cc cm}^{-2} \text{ kyr}^{-1}$ over Contessa Cycle B and $9.0 \pm 1.8 \times 10^{-14} \text{ cc cm}^{-2} \text{ kyr}^{-1}$ over Furlo Cycle C. These figures are similar to the background flux values over this interval calculated by Farley *et al.* (2012) from $^3\text{He}_{\text{ET}}$ concentrations measured in spot samples and using average sedimentation rates in the Scaglia Bianca estimated between biostratigraphic tie-points (Fig. 8, average background flux of $4.4 \pm 1.4 \times 10^{-14} \text{ cc cm}^{-2} \text{ kyr}^{-1}$). Because precession cycles represent extremely short snapshots of time within the overall span from which the cycles were collected, an overall average value of background flux may not be the best

representation of the actual flux during a given snapshot; fluctuation of background flux values on the order of *ca* 30 to 70% (1σ) on *ca* 100 kyr timescales is a common feature of $^3\text{He}_{\text{ET}}$ records (Mukhopadhyay *et al.*, 2001a,b; Farley & Eltgroth, 2003; Murphy *et al.*, 2010; Farley *et al.*, 2012).

Extraterrestrial helium abundance ($^3\text{He}_{\text{ET}}$) age models

Instantaneous sedimentation rates were calculated for each bed within the studied precession cycles using the following relationship, reflecting the dilution of extraterrestrial-helium-bearing interplanetary dust particles (IDPs) by other sediment (Takayanagi & Ozima, 1987): $\alpha = F / [^3\text{He}_{\text{ET}}]$, where α is the accumulation rate of sediment ($\text{g cm}^{-2} \text{ year}^{-1}$), $[^3\text{He}_{\text{ET}}]$ is the concentration of extraterrestrial ^3He (cc g^{-1}) and F is the background flux of extraterrestrial ^3He into sediments ($\text{cc cm}^{-2} \text{ year}^{-1}$). A background flux value specific to each cycle, as discussed above, was used in this equation. Calculated linear sedimentation rate, carbonate accumulation rate, organic-carbon mass accumulation rate and terrestrial ^4He flux through the precession cycles are presented in Fig. 9.

Carbonate accumulation rates were calculated from mass accumulation rate (α) and carbonate content calculated from Rock-Eval measurements of inorganic (mineral) carbon: carbonate $\text{MAR} = \alpha \times \text{carbonate content (\%)}$. Organic-carbon mass accumulation rates (OC MAR) were calculated in a similar manner using TOC content from Rock-Eval measurements: $\text{OC MAR} = \alpha \times \text{TOC (\%)}$. Linear sedimentation rates were calculated from measured $^3\text{He}_{\text{ET}}$ concentration using the cycle-specific background flux (F_{cycle}) and an average dry bulk density for the Scaglia Bianca lithologies of $2.7 \pm 0.5 \text{ g cm}^{-3}$ (Mukhopadhyay *et al.*, 2001b; Chicco *et al.*, 2019): $\text{LSR} = F_{\text{cycle}} / ([^3\text{He}_{\text{ET}}] \times \text{density})$. This density value lies within the range of typical ‘older’ shales (2.65 to 2.75 g cm^{-3} , Sharma, 1997) and measured cherts (2.24 to 2.74 g cm^{-3} , Tenzer *et al.*, 2011). The effect of expected density variation on calculated linear sedimentation rates is minor compared to impact of uncertainties in $^3\text{He}_{\text{ET}}$ concentration due to the nugget effect.

It should be noted that these ‘linear sedimentation rates’ relate to the rock in outcrop and are, therefore, a result not only of the rate of accumulation of sedimentary components in the Cenomanian Tethys, but also post-depositional

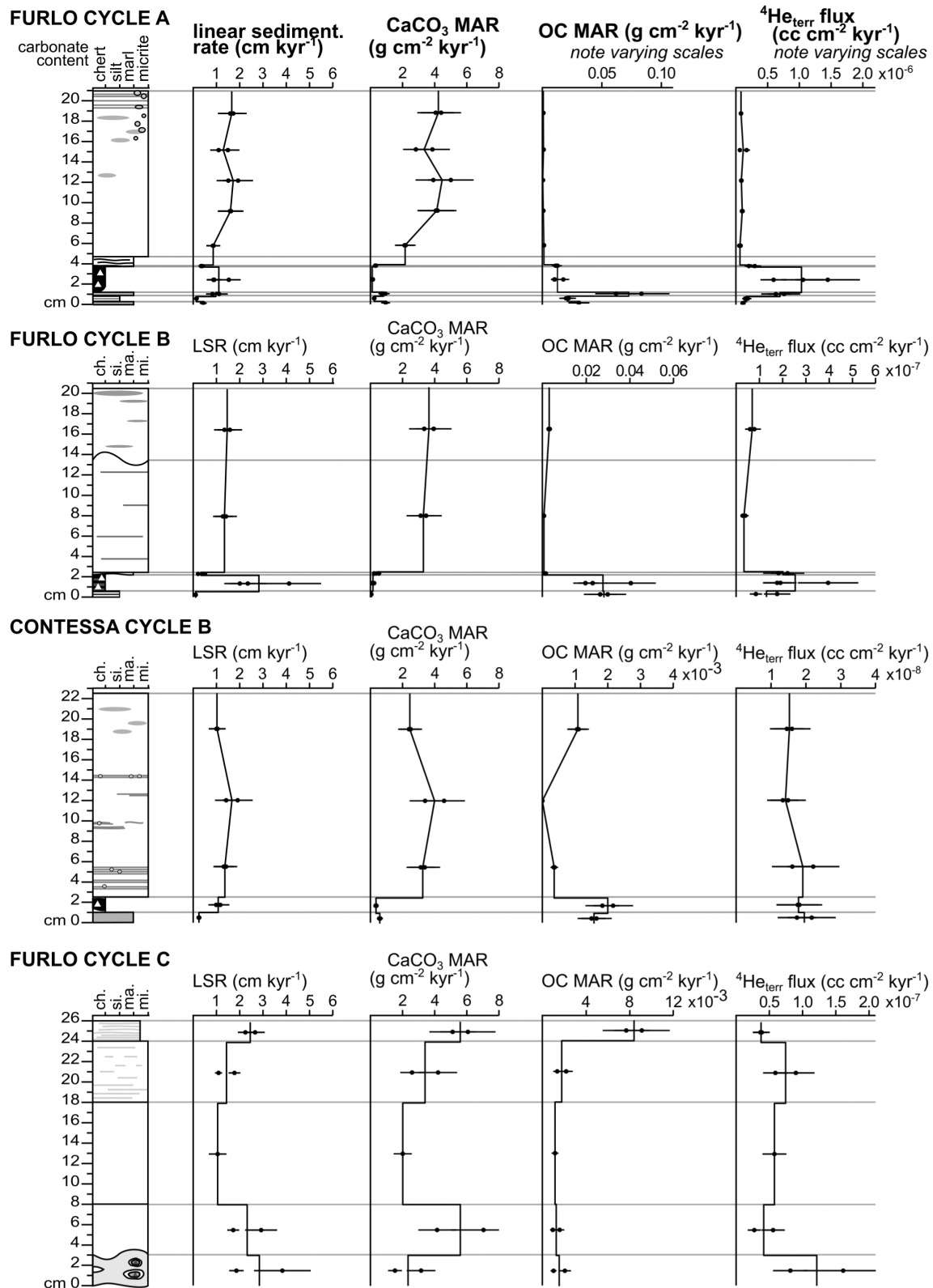


Fig. 9. Linear sedimentation rate, carbonate mass accumulation rate, organic-carbon mass accumulation rate and flux of terrestrial ⁴He through the studied precession cycles. Data points represent individual measurements; solid lines represent average values. Error bars represent total uncertainty, the largest contributor to which is the uncertainty on background flux used to calculate accumulation rate. For legend see Fig. 7.

compaction, along with any diagenetic effects, such as early lithification or pressure solution, that act to increase or decrease the thickness of a bed (cf. Bathurst, 1987). Despite this complexity, sedimentation rates remain a useful tool, being particularly meaningful when comparing two beds of the same lithology that might be assumed to have similar diagenetic histories, but also allowing different lithologies to be contrasted.

Sub-Bonarelli black shales represent the periods of slowest deposition within the precession cycles, with sedimentation rates of $0.14 \pm 0.02 \text{ cm kyr}^{-1}$ in Furlo Cycle A and $0.10 \pm 0.01 \text{ cm kyr}^{-1}$ in Furlo Cycle B (see Fig. 9). Slowly deposited beds in the Furlo cycles appear to be TOC-rich and carbonate-poor. Although there is no appreciable difference in the TOC content between the marl beneath the black chert of Contessa Cycle B and the limestones that underlie it, the sedimentation rate in the marl bed is considerably lower than the typical value of homogenous limestone ($0.25 \pm 0.04 \text{ cm kyr}^{-1}$ compared to $1.29 \pm 0.18 \text{ cm kyr}^{-1}$), confirming a pattern in Cycle B at both localities of a slower depositing bed (of black shale at Furlo and marl at Contessa) beneath the chert layers. Sedimentation rates in the black cherts of

these cycles, $1.10 \pm 0.48 \text{ cm kyr}^{-1}$ in Furlo Cycle A, $2.80 \pm 1.12 \text{ cm kyr}^{-1}$ in Furlo Cycle B and $1.07 \pm 0.28 \text{ cm kyr}^{-1}$ in Contessa Cycle B, are notably faster than those in the underlying black shales or marl (the other 'black bed' lithologies). Significant differences in sedimentation rate are, by contrast, not observed across the limestones and grey chert of Furlo Cycle C.

The average sedimentation rates of the limestones are very similar across the three cycles ($1.32 \pm 0.15 \text{ cm kyr}^{-1}$, Furlo Cycle A; $1.26 \pm 0.20 \text{ cm kyr}^{-1}$, Furlo Cycle B; $1.29 \pm 0.18 \text{ cm kyr}^{-1}$, Contessa Cycle B; $1.11 \pm 0.07 \text{ cm kyr}^{-1}$, Furlo Cycle C). Sedimentation rates do not appear to vary much through the homogenous limestone beds. This similarity may be because these beds were all deposited at a uniform rate. However, the effects of bioturbation have almost certainly homogenized this signal such that it is impossible to conclude anything about intra-bed variability.

Precession cycle logs plotted against time are presented in Fig. 10. It is worth noting here that the calculation of time spanned by a bed relates to its total extraterrestrial helium content. Although bed thickness (and therefore helium concentration) is likely to be affected by differential compaction or diagenetic effects, total

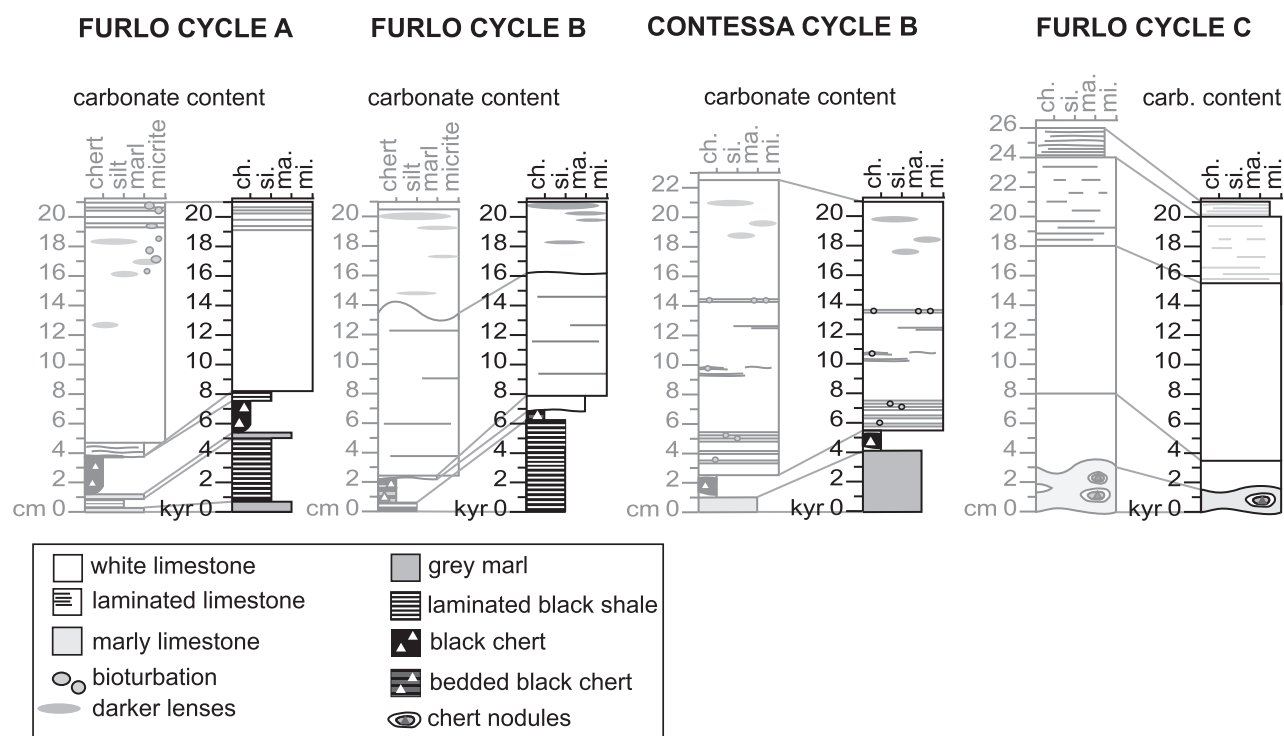


Fig. 10. Precession cycle logs against time.

extraterrestrial helium content is not affected by these processes, allowing many of the complexities involved in the interpretation of 'sedimentation rate' and its relationship to the contemporary 'at-the-seafloor' accumulation rate of sedimentary components to be set aside.

Table 1 summarizes the time represented by each lithology in the studied precession cycles, assuming a total duration for each precession cycle of 21 kyr (see above). Limestone accounts for 61 to 90% of these precession cycles by time, and was deposited over a notably smaller proportion of Furlo Cycles A and B than Furlo Cycle C, with the proportion of limestone by time in Contessa Cycle B falling between these two extremes but comparable to Furlo Cycle B. In cycles containing black shales, this lithology comprises *ca* 25 to 29% of the precession cycle by time; the slower depositing marl beneath the black chert in Contessa Cycle B comprises a comparable *ca* 19%. Chert beds occupy between *ca* 3% and *ca* 11% of the precession cycles by time.

Because Furlo and Contessa Cycles B were deposited synchronously, the proportion of time spanned by each lithology therein might be expected to be the same. As seen in Table 1, the two time spans of the 'homogenous' limestones are indeed within error of one another in the two cycles, as is the time spanned by black shale (in Furlo) and marl (in Contessa). The time spanned by the black chert beds of the two cycles is, however, somewhat outside error, with

the black chert bed in Furlo apparently deposited over less time than the chert bed in Contessa (see further discussion of chert beds within $^3\text{He}_{\text{ET}}$ -timescales below).

Mechanisms of chert formation and their effects on a $^3\text{He}_{\text{ET}}$ timescale

When considering 'sedimentation rates' and 'depositional durations' of chert beds in these cycles it is important to remember that chert is a diagenetic, rather than primary, sedimentary lithology. Figure 11 presents various mechanisms under which the interplay between diagenesis and changes in primary sedimentation could result in the stratigraphy observed in the Scaglia Bianca.

It is judged likely that the position of chert relative to limestone beds reflects a change in primary lithology, because the chert beds are tabular and laterally continuous, rather than nodular; furthermore, silicified foraminifera within the cherts indicate that they do not simply represent times of greatly increased carbonate dissolution (Arthur & Premoli Silva, 1982; Mitchell *et al.*, 2008; Batenburg *et al.*, 2016; Gambacorta *et al.*, 2016). The presence of foraminifera and radiolaria infilled with silica in limestone beds that overlie cherts does, however, confirm some movement of siliceous fluids through carbonate ooze in the Scaglia Bianca. This may be very local movement of silica

Table 1. Proportion of time occupied by each lithology within the studied precession cycles, presented as time occupied within a 21 kyr precession cycle and % of cycle. Uncertainties derive from uncertainties in measured $^3\text{He}_{\text{ET}}$ concentration, with contributions from uncertainty in measured bed thickness and estimated density.

Lithology	Cycle	Time occupied within cycle (%)	Time occupied within 21 kyr precession cycle (kyr)
'Homogenous' limestone	Furlo Cycle A	61 ± 7	12.8 ± 1.4
	Furlo Cycle B	68 ± 11	14.3 ± 2.3
	Contessa Cycle B	74 ± 10	15.6 ± 2.1
	Furlo Cycle C	90 ± 6	18.9 ± 1.2
'Laminated' limestone	Furlo Cycle C	4 ± 1	0.8 ± 0.2
Marl below chert	Contessa Cycle B	19 ± 5	4.0 ± 1.0
Black shale below chert	Furlo Cycle A	25 ± 5	5.2 ± 1.1
	Furlo Cycle B	29 ± 7	6.1 ± 1.5
Black shale above chert	Furlo Cycle A	3 ± 1	0.6 ± 0.2
Chert	Furlo Cycle A	11 ± 3	2.4 ± 0.6
	Furlo Cycle B	3 ± 1	0.6 ± 0.1
	Contessa Cycle B	7 ± 2	1.4 ± 0.3
	Furlo Cycle C	6 ± 1	1.2 ± 0.3

What does the division of chert and black shale represent?

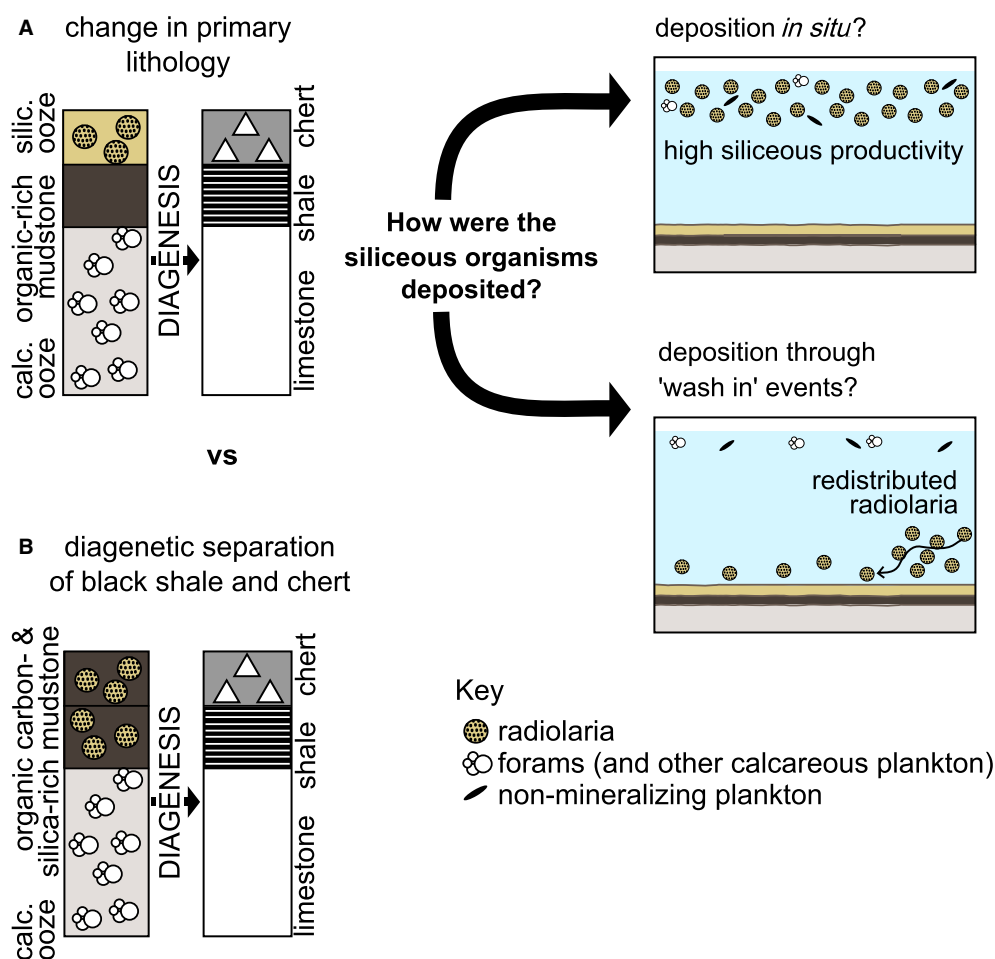


Fig. 11. Summary of postulated methods (Scenarios A and B) of the formation of chert and black shale beds in the Scaglia Bianca.

deposited within the carbonate ooze, because no macroscopic evidence of silica migration, for example, quartz veining, was observed in the studied sections. Conversely, dissolved silica may manifestly move through metres of host sediments along concentration gradients to concentrate in cherts (Knauth, 1979; Bromley & Ekdale, 1986; Clayton, 1986; Hesse, 1989).

Abundant preserved 'ghost' radiolarians in chert beds suggest that if the chert and shale beds represent different primary lithologies (scenario 'A' in Fig. 11), the proto-chert may have been a radiolarian sand. Assuming that the limits of the chert beds roughly correspond to the limits of the 'original' radiolarian sand, deposition of these beds took place over a period of between *ca* 600 and 2400 years. This

time span may represent the duration of high *in situ* biosiliceous productivity conditions, or the period within which a series of radiolarian wash-in events occurred, perhaps overlying a slow background deposition of black shale: an interpretation of 'bedded black cherts' put forward by Gambacorta *et al.* (2014, 2016).

If redistribution of radiolarian skeletons occurred within the Umbria–Marche Basin, a key question is whether this process was accompanied by redistribution of $^3\text{He}_{\text{ET}}$ -bearing particles, and hence an alteration of the relationship between measured $^3\text{He}_{\text{ET}}$ concentration and duration of deposition in redeposited beds. Redistribution of radiolarians is suggested to have occurred both during their production in the surface water and vertical transport through

the water column and, post-depositionally, their transport being made easier by their relatively low density and high surface area (Gambacorta *et al.*, 2014). The hydrographic properties of radiolaria make them more likely to be redistributed than $^3\text{He}_{\text{ET}}$ -bearing particles. By contrast, because most $^3\text{He}_{\text{ET}}$ -bearing particles are in the 1 to 10 μm size fraction (Brook *et al.*, 2009; McGee *et al.*, 2010; Torfstein, 2012), due to flocculation they are likely to have been laid down as larger aggregates as well as being more difficult to remobilize once deposited, making them less prone to redistribution (Curran *et al.*, 2004; McCave & Hall, 2006). Extraterrestrial ^3He is also suspected to be hosted in magnetite, or an associated phase, so $^3\text{He}_{\text{ET}}$ -bearing particles are also likely to have been of relatively high density compared to radiolaria (Mukhopadhyay & Farley, 2006). In a study of Quaternary sediments in the North Atlantic, McGee *et al.* (2010) found that, even in settings with extreme sediment redistribution, $^3\text{He}_{\text{ET}}$ -based sedimentation rates were minimally affected. The co-existence of redistribution of radiolaria with an undisturbed $^3\text{He}_{\text{ET}}$ timescale is therefore not unreasonable; a 'wash in' of radiolaria in one location might have inflated the apparent sedimentation rate, but $^3\text{He}_{\text{ET}}$ timescales would still provide the interval of time over which 'blooms' of radiolaria occurred somewhere in the basin, even if their skeletal remains were subsequently redeposited, reflecting overall a change in oceanographic conditions at the time to those favouring siliceous production and preservation.

The chert–shale division between carbonate-poor beds may have been instead a result of diagenetic separation (scenario 'B' in Fig. 11). This process has been suggested to result in chert/shale or chert/marl 'couplets' in various sequences globally, including the Scaglia Bianca and Scaglia Rossa (Murray *et al.*, 1992; Salmon *et al.*, 2003; Trabucchi-Alexandre *et al.*, 2011; Abrajvitch, 2020), as well as the varied TOC content measured in black shales of the same stratigraphic level (see Jenkyns *et al.*, 2007; Owens *et al.*, 2017). If diagenetic separation alone controlled the distinction between cherts and shales, 'the sub-Bonarelli black shales' must be considered as a distinctive unit in their own right.

Distinguishing between primary lithological change and diagenetic unmixing as the mechanisms for the formation of Scaglia Bianca black cherts and black shales (scenarios 'A' and 'B') is very difficult with the existing data. The differing sedimentation rates measured in cherts and black

shales are also not necessarily incompatible with the process of diagenetic separation: diagenesis of the cherts at an early stage of sedimentary compaction (Salmon *et al.*, 2003) could have resulted in an elevated linear sedimentation rate (cm kyr^{-1}) in comparison to more compacted shales derived from the same original primary lithology. Black shales underlying black cherts are, like the cherts themselves, radiolarian-rich, and the markedly lower organic-carbon content in black cherts may be explained by oxidative destruction during diagenesis (Salmon *et al.*, 2003). The presence of planktonic foraminifera in black shales, but not cherts, might be explained by replacement of carbonate during chertification (Knauth, 1994), though the 'ghosts' of foraminifera have frequently been recorded alongside those of radiolaria in cherts from other formations (e.g. Heath & Moberly, 1971; von der Borch *et al.*, 1971), perhaps lending significance to their absence in the Scaglia Bianca cherts as reflecting a difference in primary lithology. Further evidence that the distinction between chert and shale beds represents a difference in primary lithology is the discovery in thin-section of a compositionally distinct layer containing markedly less organic matter (Fig. 5E and F) stratigraphically between the two sediment types. Neither primary lithological change nor diagenetic unmixing can be entirely ruled out to explain the pattern of black shale and chert layers which may, indeed, be partly a result of both processes.

In some settings, alternations of marl and limestone are believed to have a diagenetic origin, or at least to have been significantly diagenetically enhanced, as a result of redistribution of carbonate (e.g. Frank *et al.*, 1999; Munnecke *et al.*, 2001; Nohl *et al.*, 2021). Examination of $^3\text{He}_{\text{ET}}$ concentrations in the NCF ($[^3\text{He}_{\text{ET}}]/\text{NCF}$) across the studied cycles reveals that, although $[^3\text{He}_{\text{ET}}]/\text{NCF}$ is within error between the limestones/black shale and limestone/marl of Furlo Cycles A and C, distinctly different $[^3\text{He}_{\text{ET}}]/\text{NCF}$ values are observed in the limestone/black shale and limestone/marl of Furlo Cycle B and Contessa Cycle B ($1.71 \pm 0.15 \times 10^{-13} \text{ cc g}^{-1}$ versus $3.41 \pm 0.48 \times 10^{-13} \text{ cc g}^{-1}$ and $0.74 \pm 0.17 \times 10^{-13} \text{ cc g}^{-1}$ versus $3.41 \pm 0.48 \times 10^{-13} \text{ cc g}^{-1}$, respectively). This result is incompatible with a dominantly diagenetic origin of lithological differences, indicating different primary lithologies for limestones versus black shales/marls, with slower deposition of the NCF in black shale/marl beds. This result affirms the previous linkage of limestone–marl alterations in the Scaglia Bianca to astronomical forcing (Batenburg *et al.*, 2016).

Carbonate mass accumulation rates, organic-carbon mass accumulation rates and primary productivity

Calculated mass accumulation rates (MARs) of carbonate in Furlo Cycles A and B and Contessa Cycle B are distinctly higher in limestone beds than in marls, black shales or cherts, though variation of carbonate accumulation rate within each cycle's limestone beds is largely within error (Fig. 9). A small proportion of inorganic diagenetic calcite notwithstanding, the majority of carbonate material in Scaglia Bianca limestones originates from primary bioproductors: planktonic foraminifera and coccoliths (Bernoulli & Jenkyns, 1974; Coccioni & Galeotti, 2003; Gambacorta *et al.*, 2014; Turpin *et al.*, 2012). Lower carbonate accumulation rates in marl, shale and chert intervals therefore suggest lower carbonate planktonic productivity at the time of their deposition.

Organic-carbon mass accumulation rates (OC MARs) through the studied precession cycles were calculated using $^3\text{He}_{\text{ET}}$ -derived sedimentation rates (Fig. 9). OC MARs in the limestones are similar across all four cycles, 0.5 to $1.9 \text{ mg cm}^{-2} \text{ kyr}^{-1}$, reflecting similar sedimentation rates and consistently low TOC. Organic-carbon mass accumulation rates peaked during the deposition of black cherts and shales; in the black cherts of Furlo Cycles A and B organic carbon accumulated at a rate of 13 to $28 \text{ mg cm}^{-2} \text{ kyr}^{-1}$, and in the black shales at a rate of 21 to $28 \text{ mg cm}^{-2} \text{ kyr}^{-1}$. OC MARs are lower in the black chert of Contessa Cycle B (*ca* $2.0 \text{ mg cm}^{-2} \text{ kyr}^{-1}$) and its underlying marl (*ca* $1.6 \text{ mg cm}^{-2} \text{ kyr}^{-1}$) than in the corresponding Furlo Cycle, reflecting the fact that overall organic-carbon content is lower at Contessa. Although black shales, where present, have a much high TOC% than the black cherts (Fig. 4), their much slower sedimentation rate means that overall OC MARs are similar between the two lithologies. Grey cherts do not appear to display such elevated OC MARs: the OC MAR measured in the grey chert of Furlo Cycle C (*ca* $1.5 \text{ mg cm}^{-2} \text{ kyr}^{-1}$) is very similar to that measured in the limestones of this cycle. The highest OC MAR recorded in these precession cycles ($74 \pm 15 \text{ mg cm}^{-2} \text{ kyr}^{-1}$) is actually seen in a marl bed in Furlo Cycle A, which has both relatively high TOC% and a faster sedimentation rate than the underlying black shale.

Elevated organic-carbon accumulation rates observed in black shales and cherts indicate that

the TOC enrichment of these beds was controlled by factors other than variable dilution by carbonate. Enhanced preservation under dysoxic conditions was likely to have played a role, as also was an increase in primary productivity (De Boer, 1982, 1991; Herbert & Fischer, 1986; Premoli Silva *et al.*, 1989; Mitchell *et al.*, 2008; Batenburg *et al.*, 2016; Gambacorta *et al.*, 2016). The correlation between elevated OC MAR and low carbonate flux (Fig. 9) may reflect a shift in the planktonic ecosystem away from calcareous plankton and towards non-mineralizing phytoplankton during the deposition of TOC-rich beds (Margalef, 1978; Premoli Silva *et al.*, 1999; Leckie *et al.*, 2002; Erba, 2004; Erba & Tremolada, 2004).

Estimating organic-carbon primary productivity from calculated OC MARs is, however, not straightforward, because the degree of organic-carbon preservation is unknown and is sensitive to multiple factors, including changes in redox conditions, type of organic matter deposited and bulk accumulation rate (e.g. Müller & Suess, 1979; Bralower & Thierstein, 1987; Canfield, 1994; Aller, 2014). Appropriate organic-carbon preservation factors may be estimated using studies of modern sedimentary systems as analogues (e.g. Pratt & King, 1986). Appropriate organic-carbon preservation factors for the varying lithologies of the Scaglia Bianca precession cycles were estimated from Aller's (2014) collation of modern measurements across a range of marine settings. Percentage of export organic carbon preserved for each lithology type was estimated using its average bulk mass accumulation rate, taking the 'normal marine' field as an analogue for limestones and grey chert, and the 'O₂-depleted' field as an analogue for black chert and black shale (Fig. 12). After the application of a further 30% reduction to these estimated C_{org} preservation factors, in order to account for later diagenetic organic-carbon loss (following Berner, 1982; Bralower & Thierstein, 1984; Pratt & King, 1986), export carbon productivity was estimated for each lithology and converted into primary productivity using the relationship of Eppley & Peterson (1979): primary productivity = (export productivity/0.0025)^{0.5} (where total primary productivity < $200 \text{ gC m}^{-2} \text{ year}^{-1}$).

Estimated primary productivity values for the varying lithologies of the Scaglia Bianca precession cycles at Furlo are presented in Table 2. Even accounting for the spread of organic-carbon preservation factors associated with a given bulk MAR, and variation in measured OC MAR, there appears to be a clear difference

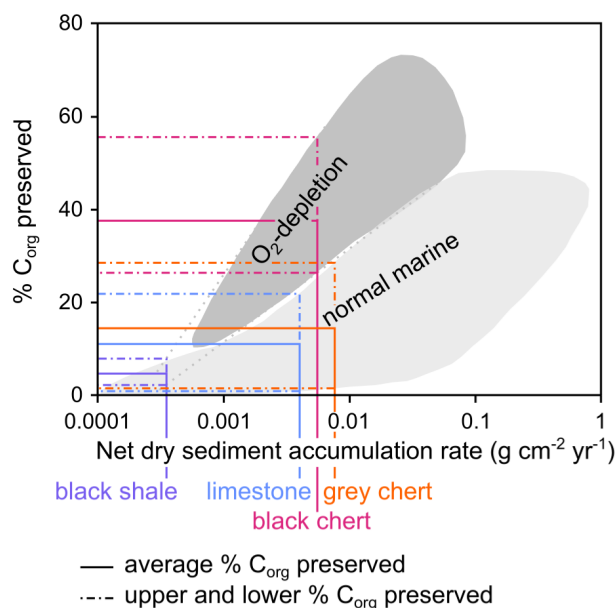


Fig. 12. Estimated average C_{org} preservation factors for lithologies from Scaglia Bianca precession cycles at Furlo, using broad fields representing the relationship between the percentage of C_{org} deposited on the seafloor that is subsequently preserved and bulk mass accumulation rate of the sediment in different depositional environments, from Aller (2014).

in primary productivity between limestones and black shales (3 to $28\ gC\ m^{-2}\ year^{-1}$ and 36 to $117\ gC\ m^{-2}\ year^{-1}$, respectively). This difference suggests that conditions of enhanced organic-carbon productivity likely contributed, along with dysoxic seafloor conditions, to the relatively higher organic-carbon mass accumulation rates recorded in black shales. Primary productivity estimated in both grey and black chert beds (6 to $24\ gC\ m^{-2}\ year^{-1}$ and 11 to $21\ gC\ m^{-2}\ year^{-1}$) is similar to that estimated in limestones; it appears that, in precession cycles containing grey cherts (interpreted as occurring at eccentricity minima), conditions conducive to higher productivity did not develop. All of these productivity estimates fall, however, within the range of expected values for 'low productivity regions' in modern oceans (Eppley & Peterson, 1979; Demaison & Moore, 1980; Falkowski *et al.*, 1998), so it is more appropriate to describe the primary productivity during black shale deposition as 'higher' rather than 'high'.

Whether higher primary productivity in the sub-Bonarelli black shales was accompanied by a shift in the type of organic matter deposited is difficult to say. Although higher Hydrogen Index

values are observed in black shales than in limestones (Fig. 6), this trend is likely to be entirely preservational: better preservation of high-HI organic matter is typically correlated with the total organic-carbon content of sediments (Hartman-Stroup, 1987; Bouloubassi *et al.*, 1999).

Terrestrial input – variations in the flux of terrestrial 4He

The $^4He_{terr}$ flux measured in limestones is fairly consistent across all three Furlo cycles (*ca* 5 to $9 \times 10^{-8}\ cc\ cm^{-2}\ kyr^{-1}$), with slightly lower values measured in limestones from the Contessa quarry (*ca* $2 \times 10^{-8}\ cc\ cm^{-2}\ kyr^{-1}$). Evident in both Furlo Cycles A and B is a spike in the flux of terrestrially derived 4He , which increases by around an order of magnitude, coincident with chert occurrences (see Fig. 9), with $^4He_{terr}$ flux reaching values of $10.3 \pm 2.1 \times 10^{-7}\ cc\ cm^{-2}\ kyr^{-1}$ and $2.5 \pm 0.5 \times 10^{-7}\ cc\ cm^{-2}\ kyr^{-1}$, respectively. This geochemical anomaly may represent a change in the source region of terrigenous material to one whose rocks contain higher concentrations of 4He : a change in the provenance of clay minerals between limestones and cherts has, for example, been observed in the Scaglia Rossa (which stratigraphically overlies the Scaglia Bianca but is lithologically similar), interpreted as a result of orbitally forced changes in climate and terrestrial weathering (Trabucchi-Alexandre *et al.*, 2011).

Higher $^4He_{terr}$ flux may also represent a transient increase in terrestrial input during the deposition of cherts. Under the 'monsoonal' model, cherts are thought to have been deposited at times of increased fertility corresponding to a strong monsoon (Mitchell *et al.*, 2008; Batenburg *et al.*, 2016; Gambacorta *et al.*, 2016, 2019). That these periods of increased productivity were coincident with periods of elevated $^4He_{terr}$ flux may be indicative of a common driver for both phenomena: namely, an increase in terrigenous input that provided both nutrients and $^4He_{terr}$ -bearing sediment to the basin. There is, however, no intrinsic reason to suppose that $^4He_{terr}$ and terrestrially sourced nutrients were necessarily delivered by the same processes; $^4He_{terr}$ is hosted in sediment and so must be delivered as terrigenous clastics (Takayanagi & Ozima, 1987; Farley, 2001; Torfstein, 2012), unlike many major nutrients that control ocean fertility, such as silica and phosphorus, which may be delivered fluviably as dissolved species (Delaney, 1998; Tyrrell, 1999; Tréguer & De La Rocha, 2013).

Table 2. Estimated primary productivity in Furlo precession cycle lithologies. Preserved OC/export OC % was estimated using a collation of modern measurements of export carbon productivity, sedimentation rate and C_{org} preservation factor across different marine settings (Blair & Aller, 2012; Aller, 2014). Primary productivity is calculated from export carbon using the relationship of Eppley & Peterson (1979). The primary productivity range is derived from the maximum range in possible C_{org} preservation factor from measured OC MAR, and the broad fields of Aller (2014).

	Average MAR (g cm ⁻² kyr ⁻¹)	Average OC MAR (mgC cm ⁻² kyr ⁻¹)	Preserved OC/export OC (%)	Preserved OC/export OC after 30% diagenetic loss (%)	Export OC (gC m ⁻² year ⁻¹)	Estimated primary productivity (gC m ⁻² year ⁻¹)	Primary productivity range (gC m ⁻² year ⁻¹)
Black shale	0.32	25.0	5	4	7.10	53	36–117
Black chert	5.30	20.0	38	27	0.76	17	11–21
Limestone	4.00	1.4	11	8	0.19	9	3–28
Grey chert	7.50	1.5	14	10	0.15	8	6–24

Preserved OC/export OC % was estimated using a collation of modern measurements of export carbon productivity, sedimentation rate and C_{org} preservation factor across different marine settings (Blair & Aller, 2012; Aller, 2014). Primary productivity is calculated from export carbon using the relationship of Eppley & Peterson (1979). The primary productivity range is derived from the maximum range in possible C_{org} preservation factor from measured OC MAR, and the broad fields of Aller (2014).

One potential delivery process for terrigenous ⁴He-bearing material is aeolian transport, which has also been suggested as the mechanism for nutrient delivery to the oceans during the deposition of proto-black cherts in the Scaglia Bianca (Gambacorta *et al.*, 2019). An alternative control on ⁴He_{terr}-bearing material may have been fluvial input, perhaps as a result of increased terrestrial run-off accompanying an intensification of the hydrological cycle. However, a fluvial contribution to the Umbria–Marche Basin during the Cenomanian has been suggested to have been minimal, with only a few or (likely) ephemeral rivers on the Tethyan margin and the shielding of the deeper basin by carbonate platforms (Bernoulli & Jenkyns, 1974).

The presence of a spike in ⁴He_{terr} flux in only one of the two studied sites (Furlo) may indicate that there was some palaeoceanographic control on this signal. A difference in the palaeoceanography of the two sites has, for example, been invoked by Gambacorta *et al.* (2016) to explain the presence of sub-Bonarelli black shales at Furlo but not Contessa. This marked difference is surprising; Furlo and Contessa are separated today by only *ca* 40 km and, although the palaeolocations of the two sites were likely further apart prior to Apennine folding, this is a small distance over which to expect significant palaeoceanographic change within the Umbria–Marche Basin. The nature of this palaeoceanographic control is also not easy to pin down; this degree of heterogeneity in two neighbouring sites would not be expected in a signal governed by aeolian transport, but, equally, explanations invoking distance from a fluvially derived sediment plume (e.g. Gambacorta *et al.*, 2016) are impossible to assess without more detailed knowledge of the regional Cenomanian palaeogeography, and are also thought to be unlikely in the dominantly pelagic setting of the Scaglia Bianca. The differing ⁴He_{terr} flux records, and presence/absence of black shales between Furlo and Contessa suggest, at least, that the two sections derive from different sub-basins, with watermasses that were geochemically different during the deposition of the Scaglia Bianca.

Palaeoenvironmental thresholds – a model for understanding the observed sedimentary changes

The pattern of chert and limestone deposits that characterizes the Scaglia Bianca may be explained within the framework of palaeoenvironmental

‘thresholds’ (following Batenburg *et al.*, 2016). Extremes of precession forcing may have led to deposition of black shale and chert during minimal eccentricity (Lanci *et al.*, 2010) by enhancing stratification, scenario ‘A’ in Fig. 13, or during maximal eccentricity (Mitchell *et al.*, 2008) by increasing the seasonal contrast, scenario ‘B’ in Fig. 13. The coincidence of maximal lithological contrast with maximal eccentricity is supported by an integrated stratigraphic approach (Batenburg *et al.*, 2016) and analysis of frequency modulation (Laurin *et al.*, 2016). Under this model (summarized in scenario ‘B’, Fig. 13), black shales and cherts developed when precession cycles were at their maximum amplitudes, at times when the local palaeoceanographic system had switched into a different depositional regime. A reason for passing this ‘threshold’ may have been an increase in nutrient availability, under which conditions the largely k-strategist calcareous plankton that dominated the ‘limestone world’ were overwhelmed and replaced by r-strategist non-mineralizing phytoplankton which dominated under mesotrophic to eutrophic conditions (Margalef, 1978; Premoli Silva *et al.*, 1999; Leckie *et al.*, 2002; Erba, 2004; Erba & Tremolada, 2004). An increase in primary productivity associated with this change would also likely have resulted in an increase in zootrophic radiolaria (Gebhardt *et al.*, 2010). The depositional regime above this threshold might be described as ‘nutrient world’. The trigger condition for its development may have been the development of ‘monsoonal conditions’, with an intensification of the hydrological cycle leading to increased influx of nutrients to the oceans and increased run-off, thereby promoting the development of water-column stratification and anoxic conditions (Fiet, 1998; Mitchell *et al.*, 2008; Tiraboschi *et al.*, 2009; Batenburg *et al.*, 2016).

Under the threshold model, the palaeoceanographic system would be expected to have remained in ‘nutrient world’ for longer during eccentricity maxima (i.e. Cycles A and B), as the intensity of precessional forcing would be above the proposed ‘threshold’ for a longer period of time. Conversely, at times of eccentricity minima (i.e. Cycle C), the system might be expected to have spent longer under a regime promoting limestone deposition. Significantly, limestone was indeed deposited over a noticeably longer period in Cycle C: *ca* 19 kyr, than in Cycles A and B: 13 to 14 kyr (Table 1).

As discussed above, the division of the ‘black bed’ lithologies proposed as the lithological

expression of ‘nutrient world’ into distinct black chert and black shale may either reflect diagenetic separation or a change in original primary lithology (Fig. 11). Considering ‘black beds’ as a single unit, as in previous conceptions of ‘thresholds’ relevant to the deposition of the Scaglia Bianca (Mitchell *et al.*, 2008; Batenburg *et al.*, 2016), the interpretation of ‘threshold crossing’ is straightforward. In Furlo Cycles A and B *ca* 7 to 8 kyr, the total time spanned by ‘black beds’, was spent in conditions favourable to siliceous deposition and organic-matter preservation, with *ca* 5 kyr spent under these conditions in Contessa Cycle B if the slowly depositing marl is considered as analogous to the black shales expressed in Furlo. In Furlo Cycle C only *ca* 1.2 kyr, the time spanned by the chert, was spent depositing sediment under these conditions. Average sedimentation rates across ‘black beds’ considered as one unit (black shale and black chert) were slower than those in limestones (0.48 ± 0.07 cm kyr⁻¹, 0.37 ± 0.08 cm kyr⁻¹ and 0.46 ± 0.09 cm kyr⁻¹ in Furlo Cycles A, B and Contessa Cycle B, respectively). At Furlo, where ⁴He_{terr} flux was elevated in the black cherts of Furlo Cycles A and B, ⁴He_{terr} flux over the entire ‘black beds’ (i.e. black chert and black shale; *ca* 1.7 to 4.3×10^{-7} cc cm⁻² kyr⁻¹) also remained elevated, relative to the limestone portions of these cycles.

If, on the other hand, black shale and black chert are considered to represent two different primary lithologies, the relationship between lithological change and ‘threshold crossing’ is rather more complex. It appears that in cycles coincident with eccentricity maxima (A and B) *ca* 5 to 6 kyr was spent in a slowly depositing lithology (black shale in Furlo or marl in Contessa) prior to *ca* 0.6 to 2.0 kyr of a more siliceous lithology, thought to have been interbedded radiolarian-rich black shales and layers of sand-sized radiolaria (Gambacorta *et al.*, 2014), that would develop into a chert (Table 1). As previously discussed, in Furlo, organic-carbon productivity was comparatively elevated during deposition of black shale. By contrast, in cycles coincident with eccentricity minima (Furlo Cycle C), no slowly depositing lithology in an analogous stratigraphic position (underlying the grey chert) is evident. It is perhaps unusual that siliceous deposition was preceded by an interval of shale only in cycles coincident with eccentricity maxima. A speculative explanation for this result might be that slightly warmer waters in ‘nutrient world’ during eccentricity maxima than during eccentricity minima (and the subsequent increase in silica dissolution

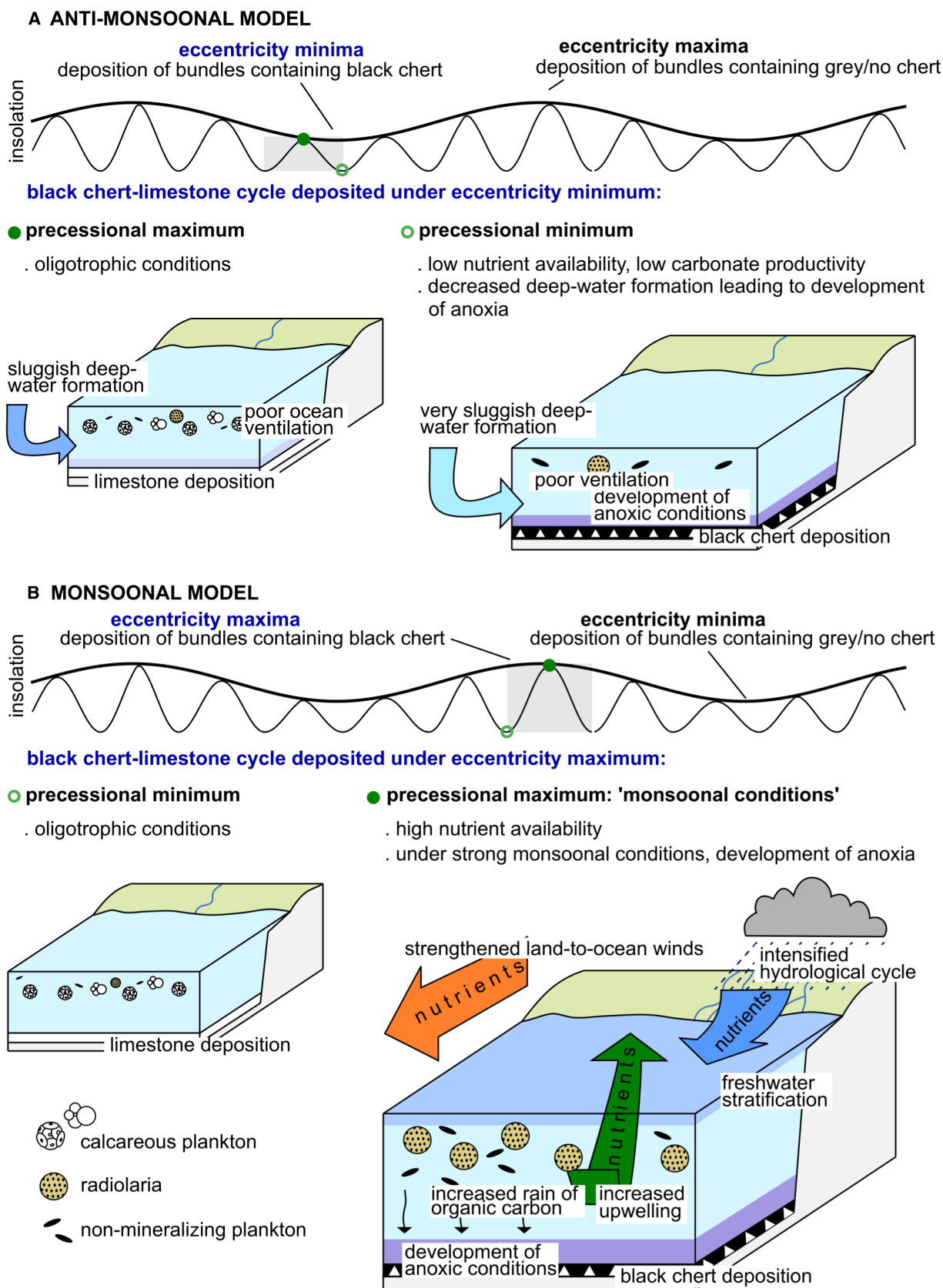


Fig. 13. Summary of 'threshold model' linking insolation forcing and the drivers of palaeoceanographic change.

in surface waters: Ragueneau *et al.*, 2000) led to black shale deposition during an interval when carbonate producers had decreased but increased siliceous production was not yet at a sufficient level to overcome dissolution in the water column or on the seafloor and be preserved within the sediment (Batenburg *et al.*, 2016; Gambacorta *et al.*, 2016). The temperature difference is, however, likely to have been very small, not more than 1° or 2° (Jarvis *et al.*, 2011); a temperature-based explanation for the observed depositional change would require a rather delicately poised system for small changes to have had such an impact, and there may be other explanations for these observed complexities.

An independent geochemical proxy for anoxic conditions, separate from productivity, was not measured in this study. However, the presence or absence of bioturbation may be used as a 'rough and ready' indicator of oxic or dysoxic conditions, as in the work of Demaison & Moore (1980) and Pratt & King (1986) in comparable Umbria–Marche successions, and global studies of organic-carbon-rich laminated sediments. Using bioturbation as an indicator, it appears that dysoxic conditions developed in 'black cycles', which contain laminated black shales and bedded black cherts, but were not as well-developed in 'grey cycles', which contain mottled grey chert without observable sedimentary structures, likely indicative of a bioturbated primary lithology. The development of anoxic conditions might be expected to have varied under different 'strengths' of precessional forcing, either due to the intensity of the forcing, or to the time over which that forcing was applied. Along with increased primary productivity and export of organic carbon to the seafloor, a major contributor to the development of anoxic conditions in these precession cycles is thought to have been stratification of the water column, either by an influx of freshwater under monsoonal conditions or by variations in surface-water temperature (Mitchell *et al.*, 2008; Tiraboschi *et al.*, 2009; Batenburg *et al.*, 2016; Gambacorta *et al.*, 2016). Stratification may have developed through a more intense hydrological cycle at a higher forcing 'peak', or through the cumulative effect of an intensified hydrological cycle over a longer period of time.

CONCLUSIONS AND IMPLICATIONS

The geological record contains multiple examples of small changes in insolation forcing during

orbital cycles that ultimately provoked dramatic lithological and geochemical shifts. By providing constraints on the rates and timescale of sedimentological changes, extraterrestrial helium abundance ($^3\text{He}_{\text{ET}}$) timescales allow the relationship between orbital forcing and environmental change to be better understood. The repeating and alternating lithological changes from cherts and black shales to limestones in the Upper Cretaceous Scaglia Bianca of Umbria–Marche, Italy, can be explained using the concept of 'palaeoenvironmental thresholds'. Cherts and organic-rich beds, facies interpreted as representing more productive conditions, comprise a larger temporal proportion of individual precession cycles during times of eccentricity maxima: an observation consistent with the idea that, as the amplitude of these precession cycles became greater, insolation values stayed above a certain 'threshold' for longer during the deposition of the facies in question. Consequently (and conversely), limestone deposition represents less time within precession cycles occurring during eccentricity maxima, compared to precession cycles occurring during eccentricity minima. The palaeoenvironmental context of this 'threshold' is proposed to be a change from dominantly calcareous to siliceous or non-mineralizing planktonic communities prompted by an increase in nutrient availability.

Using $^3\text{He}_{\text{ET}}$ concentration to calculate sedimentation rates within a precession cycle also highlights the large differences in the relationship between 'depth' and 'time' that occur through the different lithologies of these Scaglia Bianca precession cycles (and, likely, in similar lithologically heterogeneous cycles) due to varying sedimentation rates – a term encompassing the result of both contemporary rate of sediment accumulation and subsequent differential compaction. This complicating factor means that, were geochemical data to be plotted against depth as a proxy for time for cyclostratigraphic analysis, the expected orbitally forced sinusoidal signal would be stretched/shrunk with the passage through different lithologies. The work presented here thus demonstrates the potential for helium isotopes to provide novel, high-resolution insights into depositional processes and rates of environmental change in pelagic settings.

ACKNOWLEDGEMENTS

This work was funded by the NERC Doctoral Training Partnership in Environmental Research

at Oxford (NE/L002612/1). Steve Wyatt, Owen Green and Jon Wells are thanked for their technical assistance in the sample preparation and thin-sectioning laboratories at Oxford. We thank the journal reviewers for their helpful comments in improving the manuscript.

DATA AVAILABILITY STATEMENT

The data that support the findings of this study are available in the [Supplementary Material](#) of this article.

REFERENCES

- Abrajevitch, A. (2020) Diagenetic formation of bedded chert: implications from a rock magnetic study of siliceous precursor sediments. *Earth Planet. Sci. Lett.*, **533**, 116039.
- Aller, R.C. (2014) Sedimentary diagenesis, depositional environments, and benthic fluxes. In: *Treatise on Geochemistry* (Eds Holland, H.D. and Turekian, K.K.), 2nd edn, pp. 293–334. Elsevier, Oxford.
- Arthur, M.A. and Premoli Silva, I. (1982) Development of widespread organic carbon-rich strata in the Mediterranean Tethys. In: *Nature and Origin of Cretaceous Carbon-Rich Facies* (Eds Schlanger, S.O. and Cita, M.B.), pp. 7–54. Academic Press, London.
- Batenburg, S.J., De Vleeschouwer, D., Sprovieri, M., Hilgen, F.J., Gale, A.S., Singer, B.S., Koeberl, C., Coccioni, R., Claeys, P. and Montanari, A. (2016) Orbital control on the timing of oceanic anoxia in the Late Cretaceous. *Clim. Past.*, **12**, 1995–2009.
- Bathurst, R.G.C. (1987) Diagenetically enhanced bedding in argillaceous platform limestones: stratified cementation and selective compaction. *Sedimentology*, **34**, 749–778.
- Beaudoin, B., M'Ban, E.P., Montanari, A. and Pinault, M. (1996) Lithostratigraphie haute résolution (< 20 ka) dans le Cénomani du bassin d'Ombrie-Marches (Italie). *CR Acad. Sci. Paris Série*, **2**, 689–696.
- Behar, F., Beaumont, V. and Pentead, H.L.D.B. (2001) Rock-Eval 6 technology: performances and developments. *Oil Gas Sci. Technol.*, **56**, 111–134.
- Berger, A. and Loutre, M.F. (1994) Astronomical forcing through geological time. In: *Orbital Forcing and Cyclic Sequences* (Eds de Boer, P.L. and Smith, D.G.), *Spec. Publs Int. Ass. Sediment.*, **19**, pp.15–24. Blackwell Scientific Publications, Oxford, England
- Berger, A., Loutre, M.F. and Laskar, J. (1992) Stability of the astronomical frequencies over the Earth's history for paleoclimate studies. *Science*, **255**, 560–566.
- Berner, R.A. (1982) Burial of organic carbon and pyrite sulfur in the modern ocean: its geochemical and environmental significance. *Am. J. Sci.*, **282**, 451–473.
- Bernoulli, D. and Jenkyns, H.C. (1974) Alpine Mediterranean and central Atlantic Mesozoic facies in relation to the early evolution of the Tethys. In: *Modern and Ancient Geosynclinal Sedimentation* (Eds Dott, R.H., Jr. and Shaver, R.H.), *SEPM Spec. Publ.*, **19**, pp. 129–160. SEPM Society for Sedimentary Geology, Tulsa, OK, USA.
- Blair, N.E. and Aller, R.C. (2012) The fate of terrestrial organic carbon in the marine environment. *Annu. Rev. Mar. Sci.*, **4**, 401–423.
- Blard, P.-H., Suchéras-Marx, B., Suan, G., Godet, B., Tibari, B., Dutilleul, J., mezine, T. and Adatte, T. (2023) Are marl-limestone alterations mainly driven by CaCO₃ variations at the astronomical timescale? New insights from extraterrestrial ³He. *Earth Planet. Sci. Lett.*, **614**, 118173.
- Bouloubassi, I., Rullkötter, J. and Meyers, P.A. (1999) Origin and transformation of organic matter in Pliocene–Pleistocene Mediterranean sapropels: organic geochemical evidence reviewed. *Mar. Geol.*, **153**, 177–197.
- Bralower, T.J. and Thierstein, H.R. (1984) Low productivity and slow deep-water circulation in mid-Cretaceous oceans. *Geology*, **12**, 614–618.
- Bralower, T.J. and Thierstein, H.R. (1987) Organic carbon and metal accumulation rates in Holocene and mid-Cretaceous sediments: palaeoceanographic significance. In: *Marine Petroleum Source Rocks* (Eds Brook, J. and Fleet, A.J.), *Geol. Soc. Lon. Spec. Publ.*, **26**, pp. 345–369. The Geological Society, London.
- Bromley, R.G. and Ekdale, A.A. (1986) Flint and fabric in the European chalk. In: *The Scientific Study of Flint and Chert* (Eds Sieveking, G.G. and Hart, M.B.), pp. 71–82. Cambridge University Press, Cambridge.
- Brook, E.J., Kurz, M.D. and Curtice, J. (2009) Flux and size fractionation of ³He in interplanetary dust from Antarctic ice core samples. *Earth Planet. Sci. Lett.*, **286**, 565–569.
- Canfield, D.E. (1994) Factors influencing organic carbon preservation in marine sediments. *Chem. Geol.*, **114**, 315–329.
- Caricchi, C., Aldega, L. and Corrado, S. (2015) Reconstruction of maximum burial along the Northern Apennines thrust wedge (Italy) by indicators of thermal exposure and modelling. *Geol. Soc. Am. Bull.*, **127**, 428–442.
- Chicco, J.M., Verdoya, M., Giuli, G. and Invernizzi, C. (2019) Thermophysical properties and mineralogical composition of the Umbria-Marche carbonate succession (central Italy). In: *250 Million Years of Earth History in Central Italy: Celebrating 25 Years of the Geological Observatory of Coldigioco* (Eds Koeberl, C. and Bice, D.M.), *Geol. Soc. Am. Spec. Pap.*, **542**, pp. 59–67. Geological Society of America, Boulder, CO, USA.
- Clayton, C.J. (1986) Flint and fabric in the European chalk. In: *The Chemical Environment of Flint Formation in Upper Cretaceous Chalks* (Eds Sieveking, G.d.G. and Hart, M.B.), pp. 43–54. Cambridge University Press, Cambridge.
- Coccioni, R. and Galeotti, S. (2003) The mid-Cenomanian Event: prelude to OAE 2. *Palaeogeogr. Palaeoclimatol. Palaeoecol.*, **190**, 427–440.
- Cresta, S., Monechi, S. and Parisi, G. (1989) *Mesozoic-Cenozoic stratigraphy in the Umbria-Marche area: Memorie descrittive della carta geologica d'Italia*. Istituto Poligrafico e Zecca dello Stato, Rome. 182 pp.
- Curran, K.J., Hill, P.S., Schell, T.M., Milligan, T.G. and Piper, D.J.W. (2004) Inferring the mass fraction of flocc-deposited mud: application to fine-grained turbidites. *Sedimentology*, **51**, 927–944.
- De Boer, P.L. (1982) Cyclicality and the storage of organic matter in middle Cretaceous pelagic sediments. In: *Cyclic and Event Stratification* (Eds Einsele, G. and Seilacher, A.), pp. 456–475. Springer-Verlag, Berlin.
- De Boer, P.L. (1991) Pelagic black shale-carbonate rhythms: orbital forcing and oceanographic response. In: *Cycles and*

- Events in Stratigraphy* (Eds Einsele, G., Ricken, W. and Seilacher, A.), pp. 63–78. Springer-Verlag, Berlin.
- Delaney, M.L.** (1998) Phosphorus accumulation in marine sediments and the oceanic phosphorus cycle. *Glob. Biogeochem. Cycles*, **12**, 563–572.
- Demaison, G.J. and Moore, G.T.** (1980) Anoxic environments and oil source bed genesis. *AAPG Bull.*, **64**, 1179–1209.
- Eppley, R.W. and Peterson, B.J.** (1979) Particulate organic matter flux and planktonic new production in the deep ocean. *Nature*, **282**, 677–680.
- Erba, E.** (2004) Calcareous nannofossils and Mesozoic oceanic anoxic events. *Mar. Micropaleontol.*, **52**, 85–106.
- Erba, E. and Tremolada, F.** (2004) Nannofossil carbonate fluxes during the Early Cretaceous: Phytoplankton response to nutrition episodes, atmospheric CO₂, and anoxia. *Palaeoceanogr. Palaeoclimatol.*, **19**, PA1008.
- Espitalié, J., Deroo, G. and Marquis, F.** (1985) La pyrolyse Rock-Eval et ses applications. Deuxième partie. *Rev. Inst. Fr. Pét.*, **40**, 755–784.
- Falkowski, P.G., Barber, R.T. and Smetacek, V.** (1998) Biogeochemical controls and feedbacks on ocean primary production. *Science*, **281**, 200–206.
- Farley, K.A.** (2001) Extraterrestrial helium in seafloor sediments: identification, characteristics, and accretion rate over geologic time. In: *Accretion of Extraterrestrial Matter throughout Earth's History* (Eds Peucker-Ehrenbrink, B. and Schmitz, B.), pp. 179–204. Springer US, Boston, MA.
- Farley, K.A. and Eltgroth, S.F.** (2003) An alternative age model for the Paleocene–Eocene thermal maximum using extraterrestrial ³He. *Earth Planet. Sci. Lett.*, **208**, 135–148.
- Farley, K.A., Montanari, A. and Coccioni, R.** (2012) A record of the extraterrestrial ³He flux through the Late Cretaceous. *Geochim. Cosmochim. Acta*, **84**, 314–328.
- Fiet, N.** (1998) Les black shales, un outil chronostratigraphique haute résolution; exemple de l'Albien du bassins de Marches-Ombrie (Italie centrale). *Bull. Soc. Géol. Fr.*, **169**, 221–231.
- Frank, T.D., Arthur, M.A. and Dean, W.A.** (1999) Diagenesis of Lower Cretaceous pelagic carbonates, North Atlantic: Paleooceanographic signals obscured. *J. Foramin. Res.*, **29**, 340–351.
- Gambacorta, G., Bersezio, R. and Erba, E.** (2014) Sedimentation in the Tethyan pelagic realm during the Cenomanian: Monotonous settling or active redistribution? *Palaeogeogr. Palaeoclimatol. Palaeoecol.*, **409**, 301–319.
- Gambacorta, G., Jenkyns, H.C., Russo, F., Tsikos, H., Wilson, P.A., Faucher, G. and Erba, E.** (2015) Carbon- and oxygen-isotope records of mid-Cretaceous Tethyan pelagic sequences from the Umbria–Marche and Belluno Basins (Italy). *Newsl. Stratigr.*, **48**, 299–323.
- Gambacorta, G., Bersezio, R., Weissert, H. and Erba, E.** (2016) Onset and demise of Cretaceous oceanic anoxic events: The coupling of surface and bottom oceanic processes in two pelagic basins of the western Tethys. *Paleoceanography*, **31**, 2015PA002922.
- Gambacorta, G., Malinverno, A. and Erba, E.** (2019) Orbital forcing of carbonate versus siliceous productivity in the late Albian–late Cenomanian (Umbria–Marche Basin, central Italy). *Newsl. Stratigr.*, **52**, 197–220.
- Gebhardt, H., Friedrich, O., Schenk, B., Fox, L., Hart, M. and Waprich, M.** (2010) Paleooceanographic changes at the northern Tethyan margin during the Cenomanian–Turonian Oceanic Anoxic Event (OAE-2). *Mar. Micropaleontol.*, **77**, 25–45.
- Hartman-Stroup, C.** (1987) The effect of organic matter type and organic carbon content on Rock-Eval hydrogen index in oil shales and source rocks. *Org. Geochem.*, **11**, 351–369.
- Heath, G.R. and Moberly, R.** (1971) Cherts from the western Pacific. In: *Initial Reports of the Deep Sea Drilling Project* (Eds Winterer, E.L., et al.), Vol. VII, pp. 991–1007. U.S. Government Printing Office, Washington.
- Herbert, T.D. and Fischer, A.G.** (1986) Milankovitch climatic origin of mid-Cretaceous black shale rhythms in central Italy. *Nature*, **321**, 739–743.
- Hesse, R.** (1989) Silica diagenesis: origin of inorganic and replacement cherts. *Earth Sci. Rev.*, **26**, 253–284.
- Hinnov, L.A.** (2013) Cyclostratigraphy and its revolutionizing applications in the earth and planetary sciences. *Geol. Soc. Am. Bull.*, **125**, 1703–1734.
- Jarvis, I., Lignum, J.S., Gröcke, D.R., Jenkyns, H.C. and Pearce, M.A.** (2011) Black shale deposition, atmospheric CO₂ drawdown, and cooling during the Cenomanian–Turonian Oceanic Anoxic Event. *Paleoceanography*, **26**, PA3201.
- Jenkyns, H.C., Matthews, A., Tsikos, H. and Erel, Y.** (2007) Nitrate reduction, sulfate reduction, and sedimentary iron isotope evolution during the Cenomanian–Turonian oceanic anoxic event. *Paleoceanography*, **22**, PA3208.
- Knauth, L.P.** (1979) A model for the origin of chert in limestone. *Geology*, **7**, 274–277.
- Knauth, L.P.** (1994) Petrogenesis of chert. *Rev. Mineral. Geochem.*, **29**, 233–256.
- Lanci, L., Muttoni, G. and Erba, E.** (2010) Astronomical tuning of the Cenomanian Scaglia Bianca Formation at Furlo, Italy. *Earth Planet. Sci. Lett.*, **292**, 231–237.
- Laskar, J., Robutel, P., Joutel, F., Gastineau, M., Correia, A.C.M. and Levrard, B.** (2004) A long-term numerical solution for the insolation quantities of the Earth. *Astron. Astrophys.*, **428**, 261–285.
- Laskar, J., Fienga, A., Gastineau, M. and Manche, H.** (2011a) La2010: a new orbital solution for the long-term motion of the Earth. *Astron. Astrophys.*, **532**, A89.
- Laskar, J., Gastineau, M., Delisle, J.-B., Farrés, A. and Fienga, A.** (2011b) Strong chaos induced by close encounters with Ceres and Vesta. *Astron. Astrophys.*, **532**, L4.
- Laurin, J., Meyers, S.R., Galeotti, S. and Lanci, L.** (2016) Frequency modulation reveals the phasing of orbital eccentricity during Cretaceous Oceanic Anoxic Event II and the Eocene hyperthermals. *Earth Planet. Sci. Lett.*, **442**, 143–156.
- Leckie, R.M., Bralower, T.J. and Cashman, R.** (2002) Oceanic anoxic events and plankton evolution: biotic response to tectonic forcing during the mid-Cretaceous. *Paleoceanogr. Palaeoclimatol.*, **17**, 13–13–29.
- Margalef, R.** (1978) Life-forms of phytoplankton as survival alternatives in an unstable environment. *Oceanol. Acta*, **1**, 493–509.
- McCave, I.N. and Hall, I.R.** (2006) Size sorting in marine muds: processes, pitfalls, and prospects for paleoflow-speed proxies. *Geochim. Geophys. Geosyst.*, **7**, Q10N05.
- McGee, D., Marcantonio, F., McManus, J.F. and Winckler, G.** (2010) The response of excess ²³⁰Th and extraterrestrial ³He to sediment redistribution at the Blake Ridge, western North Atlantic. *Earth Planet. Sci. Lett.*, **299**, 138–149.
- Mitchell, R.N., Bice, D.M., Montanari, A., Cleaveland, L.C., Christianson, K.T., Coccioni, R. and Hinnov, L.A.** (2008) Oceanic anoxic cycles? Orbital prelude to the Bonarelli Level (OAE 2). *Earth Planet. Sci. Lett.*, **267**, 1–16.

- Mukhopadhyay, S. and Farley, K.A. (2006) New insights into the carrier phase(s) of extraterrestrial ^3He in geologically old sediments. *Geochim. Cosmochim. Acta*, **70**, 5061–5073.
- Mukhopadhyay, S., Farley, K.A. and Montanari, A. (2001a) A short duration of the Cretaceous-Tertiary boundary event: evidence from extraterrestrial Helium-3. *Science*, **291**, 1952–1955.
- Mukhopadhyay, S., Farley, K.A. and Montanari, A. (2001b) A 35 Myr record of helium in pelagic limestones from Italy: implications for interplanetary dust accretion from the early Maastrichtian to the middle Eocene. *Geochim. Cosmochim. Acta*, **65**, 653–669.
- Müller, P.J. and Suess, E. (1979) Productivity, sedimentation rate, and sedimentary organic matter in the oceans—I. Organic carbon preservation. *Deep Sea Res. Part A Oceanogr. Res. Pap.*, **26**, 1347–1362.
- Munnecke, A., Westphal, W., Elrick, M. and Reijmer, J.J.G. (2001) The mineralogical composition of precursor sediments of calcareous rhythmites: a new approach. *Int. J. Earth Sci.*, **90**, 795–812.
- Murphy, B.H., Farley, K.A. and Zachos, J.C. (2010) An extraterrestrial ^3He -based timescale for the Paleocene–Eocene thermal maximum (PETM) from Walvis Ridge, IODP Site 1266. *Geochim. Cosmochim. Acta*, **74**, 5098–5108.
- Murray, R.W., Jones, D.L. and ten Brink, M.R.B. (1992) Diagenetic formation of bedded chert: Evidence from chemistry of the chert-shale couplet. *Geology*, **20**, 271–274.
- Nier, A.O. and Schlutter, D.J. (1990) Helium and neon isotopes in stratospheric particles. *Meteoritics*, **25**, 263–267.
- Nier, A.O. and Schlutter, D.J. (1992) Extraction of helium from individual interplanetary dust particles by step-heating. *Meteoritics*, **27**, 166–173.
- Nohl, T., Steinbauer, M.J., Sinnesael, M. and Jarochowska, E. (2021) Detecting initial aragonite and calcite variations in limestone–marl alterations. *Sedimentology*, **68**, 3012–3115.
- Owens, J.D., Lyons, T.W., Hardisty, D.S., Lowery, C.M., Lu, Z., Lee, B. and Jenkyns, H.C. (2017) Patterns of local and global redox variability during the Cenomanian–Turonian Boundary Event (Oceanic Anoxic Event 2) recorded in carbonates and shales from central Italy. *Sedimentology*, **64**, 168–185.
- Ozima, M., Takayanagi, M., Zashu, S. and Amari, S. (1984) High $^3\text{He}/^4\text{He}$ ratio in ocean sediments. *Nature*, **311**, 448–450. <https://doi.org/10.1038/311448a0>
- Patterson, D.B. and Farley, K.A. (1998) Extraterrestrial ^3He in seafloor sediments: evidence for correlated 100 kyr periodicity in the accretion rate of interplanetary dust, orbital parameters, and Quaternary climate. *Geochim. Cosmochim. Acta*, **62**, 3669–3682.
- Pratt, L.M. and King, J.D. (1986) Variable marine productivity and high eolian input recorded by rhythmic black shales in Mid-Cretaceous pelagic deposits from central Italy. *Paleoceanography*, **1**, 507–522.
- Premoli Silva, I., Ripepe, M. and Tornaghi, M.E. (1989) Planktonic foraminiferal distribution record productivity cycles: evidence from the Aptian-Albian Piobbico core (central Italy). *Terra Nova*, **1**, 443–448.
- Premoli Silva, I., Erba, E., Salvini, G., Locatelli, C. and Verga, D. (1999) Biotic changes in Cretaceous oceanic anoxic events of the Tethys. *J. Foramin. Res.*, **29**, 352–370.
- Ragueneau, O., Tréguer, P., Leynaert, A., Anderson, R.F., Brzezinski, M.A., DeMaster, D.J., Dugdale, R.C., Dymond, J., Fischer, G., François, R., Heinze, C., Maier-Reimer, E., Martin-Jézéquel, V., Nelson, D.M. and Quéguiner, B. (2000) A review of the Si cycle in the modern ocean: recent progress and missing gaps in the application of biogenic opal as a paleoproductivity proxy. *Glob. Planet. Chang.*, **26**, 317–365.
- Salmon, V., Derenne, S., Lallier-Vergès, E., Connan, J., Kahn-Harari, A. and Largeau, C. (2003) Origin of compositional differences in organic matter abundance and oil potential of cherty and clayey Cenomanian black levels in the Umbria-Marche basin (Italy). *Org. Geochem.*, **34**, 1237–1245.
- Schwarzacher, W. (1994) Cyclostratigraphy of the Cenomanian in the Gubbio District, Italy; a field study. In: *Orbital Forcing and Cyclic Sequences* (Eds de Boer, P.L. and Smith, D.G.). *Spec. Publs Int. Ass. Sediment.*, **19**, 87–97. Blackwell Scientific Publications, Oxford, England.
- Sharma, V. (1997) *Environmental and Engineering Geophysics*. Cambridge University Press, Cambridge. 17 pp.
- Sprovieri, M., Sabatino, N., Pelosi, N., Batenburg, S.J., Coccioni, R., Iavarone, M. and Mazzola, S. (2013) Late Cretaceous orbitally paced carbon isotope stratigraphy from the Bottaccione Gorge (Italy). *Palaeogeogr. Palaeoclimatol. Palaeoecol.*, **379–380**, 81–94.
- Takayanagi, M. and Ozima, M. (1987) Temporal variation of $^3\text{He}/^4\text{He}$ ratio recorded in deep-sea sediment cores. *J. Geophys. Res.*, **92**, 12531–12538.
- Tenzer, R., Sirguey, P., Rattenbury, M. and Nicolson, J. (2011) A digital rock density map of New Zealand. *Comput. Geosci.*, **37**, 1181–1191.
- Tiraboschi, D., Erba, E. and Jenkyns, H.C. (2009) Origin of rhythmic Albian black shales (Piobbico core, central Italy): calcareous nannofossil quantitative and statistical analyses and paleoceanographic reconstructions. *Paleoceanography*, **24**, PA2222.
- Torfstein, A. (2012) Size fractionation, reproducibility and provenance of helium isotopes in north-equatorial pacific pelagic clays. *Earth Planet. Sci. Lett.*, **339**, 151–163.
- Trabucho-Alexandre, J., Negri, A. and de Boer, P.L. (2011) Early Turonian pelagic sedimentation at Moria (Umbria-Marche, Italy): primary and diagenetic controls on lithological oscillations. *Palaeogeogr. Palaeoclimatol. Palaeoecol.*, **311**, 200–214.
- Tréguer, P.J. and De La Rocha, C.L. (2013) The World Ocean Silica Cycle. *Annu. Rev. Mar. Sci.*, **5**, 477–501.
- Tsikos, H., Jenkyns, H.C., Walsworth-Bell, B., Petrizzo, M.R., Forster, A., Kolonic, S., Erba, E., Premoli Silva, I., Baas, M., Wagner, T. and Sinninghe Damsté, J.G. (2004) Carbon-isotope stratigraphy recorded by the Cenomanian–Turonian Oceanic Anoxic Event: correlation and implications based on three key localities. *J. Geol. Soc. Lond.*, **161**, 711–719.
- Turgeon, S. and Brumsack, H.-J. (2006) Anoxic vs dysoxic events reflected in sediment geochemistry during the Cenomanian–Turonian Boundary Event (Cretaceous) in the Umbria–Marche Basin of central Italy. *Chem. Geol.*, **234**, 321–339.
- Turpin, M., Laurent, E., Immenhauser, A. and Renard, M. (2012) Geochemical and petrographical characterization of fine-grained carbonate particles along proximal to distal transects. *Sediment. Geol.*, **281**, 1–20.
- Tyrrell, T. (1999) The relative influences of nitrogen and phosphorus on oceanic primary production. *Nature*, **400**, 525–531.
- Von der Borch, C.C., Galehouse, J. and Nesterhoff, W.D. (1971) Silicified limestone-chert sequences cored during leg 8 of the Deep Sea Drilling Project: a petrographic study. In: *Initial Reports of the Deep Sea Drilling Project*,

Vol. VIII (Eds Tracey, J.I., Jr., *et al.*), pp. 819–827. U.S. Government Printing Office, Washington.

Waltham, D. (2015) Milankovitch period uncertainties and their impact on cyclostratigraphy. *J. Sediment. Res.*, **85**, 990–998.

Zeeden, C., Meyers, S.R., Lourens, L.J. and Hilgen, F.J. (2015) Testing astronomically tuned age models. *Paleoceanography*, **30**, 369–383.

Manuscript received 20 December 2022; revision accepted 15 April 2024

Supporting Information

Additional information may be found in the online version of this article:

Data S1. Supplementary Data

Data S2. Sample preparation and laser heating method